THE JOURNAL OF PHYSICAL CHEMISTRY A

Article

pubs.acs.org/JPCA

The Many Facets of Chalcogen Bonding: Described by Vibrational Spectroscopy

Vytor Oliveira, Dieter Cremer,[†] and Elfi Kraka*

Computational and Theoretical Chemistry Group (CATCO), Department of Chemistry, Southern Methodist University, 3215 Daniel Ave, Dallas, Texas 75275-0314, United States

Supporting Information

ABSTRACT: A diverse set of 100 chalcogen-bonded complexes comprising neutral, cationic, anionic, divalent, and double bonded chalcogens has been investigated using ωB97X-D/aug-cc-pVTZ to determine geometries, binding energies, electron and energy density distributions, difference density distributions, vibrational frequencies, local stretching force constants, and associated bond strength orders. The accuracy of ωB97X-D was accessed by CCSD(T)/aug-cc-pVTZ calculations of a subset of 12 complexes and by the CCSD(T)/aug-cc-pVTZ //ωB97X-D binding energies of 95 complexes. Most of the weak chalcogen bonds can be rationalized on the basis of electrostatic contributions, but as the bond becomes stronger, covalent contributions can assume a primary role in the strength and geometry of the complexes. Covalency in chalcogen bonds involves the charge transfer from a lone pair orbital of a Lewis base into the σ* orbital of a divalent chalcogen or a π* orbital of a double bonded chalcogen. We describe for the first time a symmetric chalcogen-bonded homodimer stabilized by a charge transfer from a lone pair orbital into a π* orbital. New polymeric materials based on chalcogen bonds should take advantage of the extra stabilization granted by multiple chalcogen bonds, as is shown for 1,2,5-telluradiazole dimers.

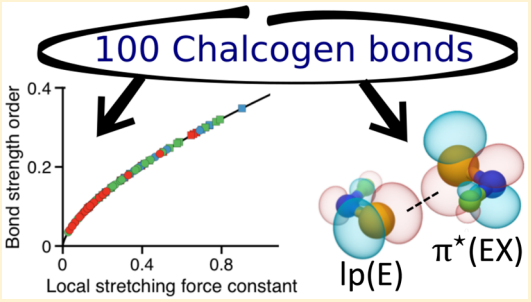

1. INTRODUCTION

Chalcogen bonding (ChB, which in the following is also used for chalcogen bond and chalcogen-bonded) is the noncovalent interaction between an electrophilic region of a chalcogen atom (S, Se, and Te) with a Lewis base in the same molecular entity (intramolecular ChB) or with another molecule (intermolecular ChB). Similar to other interactions involving the main block elements, such as halogen bonding (XB) and pnicogen bonding (PnB), the ChB is a secondary bond interaction (SBI). The term SBI was coined by Alcock in 1972[1] based on crystallographic data and is used to designate interactions that are longer than covalent bonds but shorter than the sum of the van der Waals radii of the atoms involved. SBIs typically form a close to linear angle with the covalent bond formed by the central atom (e.g., a halogen, chalcogen, or pnicogen) and its most electronegative ligand.[1−3]

Although less explored than hydrogen bonding (HB) or XB, the ChB has a great potential, with applications in a myriad of different fields. In supramolecular chemistry, ChBs are used to synthesize columnar structures,[4−6] macrocycles,[7] rotaxanes,[8] and ribbon-like polymeric structures formed by chalcogenadiazoles derivatives.[9−18] In biochemistry, ChBs are found to control to some extent the tertiary structure of several proteins, suggesting that they could be used for protein engineering.[19,20] ChBs also play key roles in biological processes. For example, the mechanism of regioselective deiodination of thyroid hormones catalyzed by selenoenzymes involves a cooperative ChB and XB.[21] Besides that, ChB finds application in catalysis[22−24] ion sensing and transport,[8,25−27] materials with nonlinear optic properties,[14,17] substrate recognition,[28] and drug design.[29−32]

Experimentally, the ChBs are accessed mostly via NMR chemical shifts and coupling constants,[8,33−36] the analysis of bond distances and angles in X-ray crystallographic structures,[2,19,20,32,37] and the analysis of UV−vis absorbance and emission spectra.[16,25,26]

Theoretical investigations on ChBs are mostly based on quantum mechanical calculations utilizing second order Møller-Plesset perturbation theory[38−51] or density functional theory (DFT),[27,43,52−56] where the accuracy of these methods are often validated by high accuracy CCSD(T) single point energy calculations of a subset of complexes.[24,48−50,57−63] These investigations were carried to better understand: (i) the ChB bonding mechanism, (ii) the dominant forces involved in the formation of the ChB, (iii) the high directionality of the ChBs,[53,64−67] (iv) the strength of the ChB and how it can be fine-tuned (v) to compare ChB with other SBIs (vi) and to support experimental analyses.

A comparison of ChB with XB, HB, PnB, or tetrel bonding was carried out by several authors.[27,53,60,68−82] The bonding mechanism of these SBIs have many common features, e.g., they all involve an electrostatic and a covalent part. The

Received: July 1, 2017
Revised: August 5, 2017
Published: August 7, 2017

DOI: 10.1021/acs.jpca.7b06479
J. Phys. Chem. A 2017, 121, 6845−6862

electrostatic part is due to a Coulomb attraction between the negative electrostatic potential at the lone pairs lp(A) or π-bond of a Lewis base and a region of positive electrostatic potential collinear to the covalent bond formed between a pnicogen (in PnB), chalcogen (in ChB) or halogen (in XB) and its most electronegative substituent (the so-called σ-hole region[64,83,84]). The covalent part is due to a charge transfer (CT) from the lp(A) orbital of the Lewis base into the σ^*(XE) orbital (E is a pnicogen (for PnB), chalcogen (for ChB) or halogen (for XB) and X is the most electronegative substituent), thus leading to a 2e-delocalization and stabilization of lp(A) (as shown on Figure 1). The magnitude of the 2e-

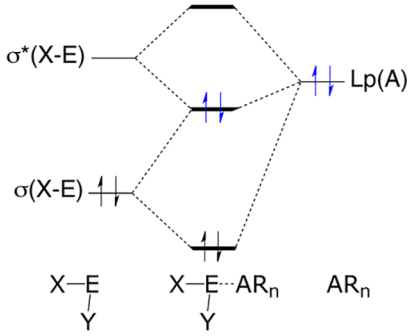

Figure 1. Peturbation molecular orbital showing the 2e-delocalization of an electron lone pair at the Ch acceptor (A) into the σ^*(XE) orbital of the Ch donor.

delocalization is proportional to lp−σ^* orbital overlap and inversely proportional to the energy gap $\Delta\epsilon$(2e) between lp(A) and the σ^*(XE) orbital. A slightly different CT mechanism can take place in sp^2 hybridized[48−50,77−79,85−88] and hypervalent chalcogens,[40,42,43,45] where charge is transferred from the lp(A) into an empty π^*(XE) orbital, which is higher in energy compared to the σ^*(XE) orbital (thus has a smaller $\Delta\epsilon$(2e) energy gap).

XBs tend to form stronger interactions than PnB or ChB, when combined with an electronegative substituents such as F.[75] However, for less electronegative substituents, ChB, PnB, and XB are of comparable strength.[43,72,74] The ChB strength can be enhanced by an anionic chalcogen donor[89] or a cationic chalcogen.[41,44,47] These strong interactions, classified as charge assisted ChBs, can have binding energies (ΔE) as high as 54.7 kcal/mol.[89]

The energy decomposition analysis of various ChB complexes, based on symmetry adapted theory (SAPT)[24,39,42,48,57,62,63,72,78] or other energy decomposition schemes[49−51,74,79,90] clearly shows that the dominant contributions to ChB are system dependent. Very weak and weak ChBs depend on an interplay between dispersion and electrostatic contributions,[38,39,48,62,78,91] whereas induction plays an essential hole in normal and strong ChBs.[42,89] Alternatively, the nature of the ChBs can be classified as covalent or electrostatic according to the electron density distribution, its Laplacian or the energy density distribution at the electron density critical bond point.[35,44,45,56,81,92]

Gleiter and co-workers[38,39] performed MP2 calculations and SAPT analyses of chalcogen bonds in X(CH_3)E···E(CH_3)$_2$ (X = CH_3, CCH or CN and E = O, S, Se, Te) complexes. From the ΔE and the interatomic distances they concluded that the ChB becomes stronger with increasing polarizability of the chalcogen atom and polarizing power of the substituent collinear to the ChB. SAPT based energy decomposition analyses showed that electrostatic contributions dominate only for complexes where one of the chalcogens is S or O.

The combination of experimental and theoretical studies led to important insights about ChB strength and nature. Tomoda and co-workers carried out a series of experimental and theoretical studies of intramolecular chalcogen bonds between Se and N, O, F, Cl, and Br heteroatoms in selenobenzyl derivatives.[33−36] The ChBs were accessed experimentally through the analysis of NMR chemical shifts and coupling constants. Binding energies were estimated by variable temperature NMR analysis. The natural bond orbital (NBO) analysis was used to describe CT. Solvents with different dielectric constants were used to evaluate the role of electrostatic contributions. They found that the strength of the ChB increases with the electron-donating ability of the heteroatoms[35] F < O < N and decreases for heavier heteroatoms[36] F > Cl > Br. Several of these ChB were considered to have a strong covalent character, with some electrostatic influence.[36] In another combined theoretical and experimental investigation Vargas-Baca and co-workers[90,93,94] performed theoretical and experimental studies on the ChBs between S, Se, Te, and N in 1,2,5-chalcogendiazole dimers. They concluded that Te···N interactions were as strong as hydrogen bonds and suitable to guide supramolecular formation. Further studies from the same group led to the development of new optically active materials based on telluradiazole derivatives.[17,95,96]

Although ΔE values and their (model dependent) decomposition into electrostatic, induction, dispersion and exchange components may provide useful information about the stabilizing forces involved in the formation of ChB complexes, they can give only a limited insight into the intrinsic strength of a bond.[75,97,98] ΔE measures the stabilization brought by complexation in an unspecific way, where the interaction between all atoms are accounted for, including secondary contributions unrelated to the atom−atom interaction of interest. ΔE is also flawed by energetic contributions from geometry and electronic relaxation processes that accompany bond dissociation. Although interatomic distances are free from these problems, they depend on the effective covalent radii of the atoms involved, which vary significantly for atoms of different periods of the periodic table (PT) and also depend on the nature of their substituents.[99−101]

A more suitable parameter capable to measure the intrinsic strength of a bond is the Konkoli−Cremer local stretching force constant,[102−104] derived from a mass-decoupled equivalent of Wilson's vibrational equation,[105] and therefore, free from mode−mode coupling. The local stretching force constant measures the curvature of the potential energy surface between the two atoms involved by applying an infinitesimally small perturbation to the bond length. Since the local stretching force constant is a second order response property, it is extremely sensitive to differences in the electronic structure (e.g., caused by changing a substituent), with the advantage that it captures only electronic effects associated with the intrinsic strength of the atom−atom interaction being analyzed.[106] The analysis of the local stretching modes and other local vibrational modes were successfully employed to investigate the strength of covalent bonds, weak interactions (such as HB, XB, PnB), and also to derive more reliable electronic parameters to describe 3c−4e bond character, aromaticity and transition metal−ligand

DOI: 10.1021/acs.jpca.7b06479
J. Phys. Chem. A 2017, 121, 6845−6862

bonds. These and other applications are summarized on Table 1.

Table 1. Previous Applications of the Local Mode Analysis

topics	references
weak bonds:	
hydrogen bonding	142−147
halogen bonding	75, 97, 148
pnicogen bonding	129, 130, 149
new electronic parameters	
aromaticity index	98, 150, 151
generalized Tolman parameter	106, 152, 153
generalized badger rule	101
covalent bonds	
the strongest bond in chemistry	122
long carbon−carbon bonds	154
carbon−halogen bonds	155, 156
bond strength bond length relationship	99−101

In the present study we will provide for the first time a quantitative analysis of the intrinsic strength of 100 ChB, aiming at answering the following questions:

(i) Can we describe the ChB mechanism and strength trends in simple but insightful terms?
(ii) How strong and covalent are the ChBs in neutral and charged complexes? Do electrostatic and covalent contributions always support each other?
(iii) How does the Lewis base influence the strength of the ChB?
(iv) How do the substituents colinear and orthogonal to the ChB affect the strength of the interactions?
(v) Can a sp^2-hybridized chalcogen form a strong ChB?
(vi) What type of molecules are more suitable for new materials based on ChB?

These questions will be addressed by the investigation of 100 neutral and charge assisted ChB complexes shown in Figure 2. In section 2, we describe all quantum-chemical tools employed in this work. The interplay between decisive electronic effects and ChB strength trends are clarified in section 3. In the last section we draw the conclusion and provide an outlook on important aspects of the ChB to be explored for the development of new materials.

The chemical structures of the ChB complexes in the present work will be denoted by X(Y)E···AR_n where X(Y)E is the chalcogen donor (Ch donor), composed of a chalcogen atom E, its X ligand collinear to the ChB, and the Y ligand orthogonal to the ChB, which will be given in parentheses. The ChB is denoted by three dots and the AR_n is the chalcogen acceptor (Ch acceptor) formed by a heteroatom A and its ligands R.

2. COMPUTATIONAL METHODS

To define a reliable method of accessible computational costs to be employed for the investigation of all 100 ChB complexes (Figure 2), the accuracy of MP2[107] and three popular exchange-correlation functionals, B3LYP-D3[108,109] (including D3(BJ) dispersion correction[110,111]), M06-2X,[112] ωB97X(-D)[113,114] (with and without empirical dispersion corrections D) was tested against CCSD(T) (coupled cluster theory including all singles, doubles and perturbative triple excitations)[115] calculated ChB distances r(EA), ΔE and ChB local stretching force constants k^a(EA) for a small set of 12 sulfur containing ChB complexes (Tables S1−S3 of the Supporting Information).

The geometry of these 12 complexes were optimized and the analytical frequencies were calculated utilizing CCSD(T) and Dunning's augmented triple-ζ basis set aug-cc-pVTZ,[116−118] which contain diffuse basis functions to describe the charge distribution of highly polarizable anions, heteroatoms, and the dispersion interactions in noncovalently bonded complexes. The ΔE values, corrected for the basis set superposition error (BSSE) employing the counterpoise correction procedure,[119] r(EA) and k^a(EA) values obtained at CCSD(T)/aug-cc-pVTZ level were then compared with MP2, B3LYP-D3, ωB97X, and ωB97X-D values. All calculations were performed with tight convergence criteria (SCF (self-consistent field), 10^{-9}; geometry iterations; forces, 10^{-6} hartree/bohr), employing aug-cc-pVTZ basis set. The DFT calculations were done with a superfine integration grid.[120]

All methods were able to reproduce CCSD(T) ΔE, r(EA) and k^a(EA) values reasonably well (Tables S1−S3). MP2 provided more accurate ΔE, whereas the long-range corrected hybrid density functional with dispersion correction ωB97X-D[113,114] had lower deviations for the r(EA) values and a smaller maximum deviation for the k^a(EA) values. Inclusion of dispersion correction in ωB97X-D improved r(EA) and k^a(EA) values but had a smaller impact on ΔE. Because of its lower computational cost compared to MP2 and its accurate r(EA) and k^a(EA) values, ωB97X-D was then picked as the method of choice to be applied for the study of the complete set of 100 ChB complexes (Figure 2).

The BSSE-corrected ΔE values of complexes **1**−**100** were calculated at the ωB97X-D/aug-cc-pVTZ(-PP) level, where relativistic effective core potentials (pseudo potentials PP) were used for Te, Se, and As.[121] For complexes **1**−**93**, the BSSE-corrected CCSD(T)/aug-cc-pVTZ(-PP)//ωB97X ΔE values were also calculated to provide an estimate of the reliability of the ωB97X-D/aug-cc-pVTZ(-PP) calculations throughout the role set (Table 2). The analysis of the local stretching force constants k^a of the ChBs was simplified by converting to bond strength orders (BSO n) using a power relationship:[101,122]

$$n = a(k^a)^b \quad (1)$$

Here the constants a = 0.372 and b = 0.657 were determined from the k^a values of two references of well-defined bond order (in the present work the NO single bond in H_2NOH with k^a = 4.497 mdyn/Å was considered to have a BSO n = 1 and the NO double bond in HNO with k^a = 12.918 mdyn/Å was considered to have a BSO n = 2). It was further assumed that a k^a of zero results in a BSO n equals to zero.

The important role of 3c−4e and other multicenter bonding mechanisms in connection with ChB was emphasized by several authors.[61,123−125] However, no quantitative assessment of the 3c−4e character of ChB complexes was made so far. Previously, we defined a quantitative parameter based on the BSO to measure the 3c−4e character of XB complexes,[75,97,98] which can easily be extended to ChBs. Considering that a 3c−4e bond is formed when the X, E and A atoms in the ChB complex adopt a symmetrical arrangement (e.g., SF_4 or SF_3^-). The three atomic orbitals involved lead to the formation of three molecular orbitals. Four electrons fill the bonding and nonbonding orbitals leaving the antibonding orbital unoccupied, resulting in XE and EA bonds of same strength and covalent character. A quantitative way to determine how close an asymmetric complex is to a symmetric 3c−4e bond situation

DOI: 10.1021/acs.jpca.7b06479
J. Phys. Chem. A 2017, 121, 6845−6862

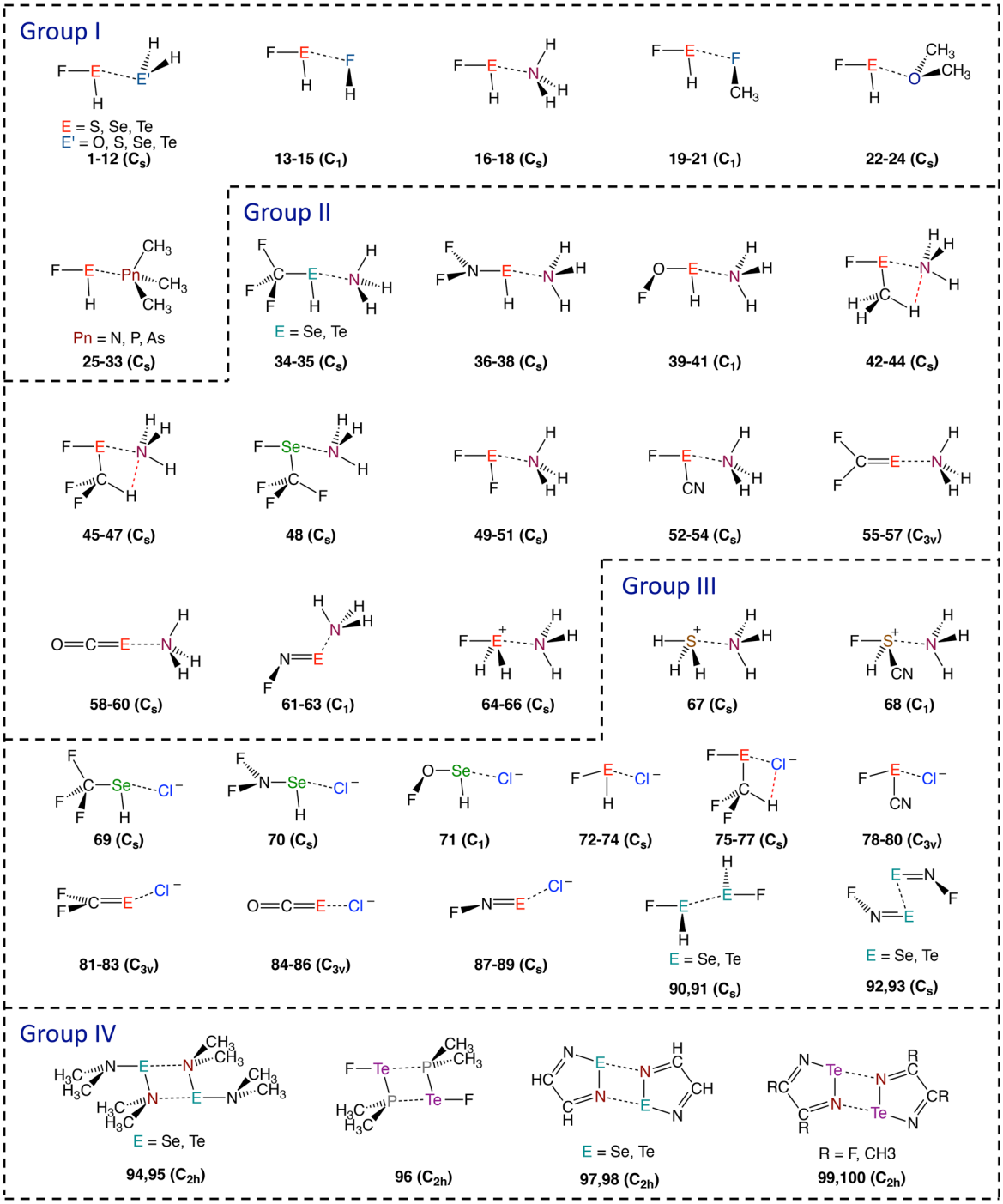

Figure 2. Schematic representation of complexes **1**−**100**.

is given by the ratio $n(XE)/n(EA) \times 100$, If this ratio leads to unity, 3c−4e bonding is fulfilled by 100%. Values smaller than 100% indicate a partial 3c−4e character.

Local properties of the electron density distribution, $\rho(\mathbf{r})$, and the energy density distribution, $H(\mathbf{r}) = G(\mathbf{r}) + V(\mathbf{r})$ ($G(\mathbf{r})$, kinetic energy density (positive, destabilizing); $V(\mathbf{r})$, potential energy density (negative, stabilizing)), were computed at the ωB97X-D/aug-cc-pVTZ(-PP) level of theory. The Cremer−Kraka criteria for covalent bonding were applied.[126−128] These associate a negative and therefore stabilizing energy density at the bond critical point $\mathbf{r}_b$ ($H(\mathbf{r}_b) = H_b < 0$) with dominant covalent character, whereas a positive (destabilizing) energy density ($H_b > 0$) is associated with a predominant electrostatic interaction.

Similar to that for PnB and XB,[75,97,129,130] the covalent character of the ChB is determined by the CT from the lp(A) of the Ch acceptor to the antibonding $\sigma^*(EX)$ orbital ($\pi^*(EX)$ for an sp^2 hybridized chalcogen) of the Ch donor, which can be assessed by calculating the NBO delocalization energy $\Delta E[\text{lp}(A) \rightarrow \sigma^*(EX)$ (or $\pi^*(EX))]= \Delta E(del)$. The magnitude of $\Delta E(del)$ was determined by second order perturbation theory.[131]

In all complexes, CT was found to involve frontier molecular orbitals (Figures S1 and S2), where the highest occupied

DOI: 10.1021/acs.jpca.7b06479
J. Phys. Chem. A 2017, 121, 6845−6862

Table 2. Summary of Energetic, Geometric, and Vibrational Data for Complexes 1−100[a]

#	complexes (sym.)	r (XE)	r (EA)	ΔE DFT	ΔE CCSD(T)	ρ_b (EA)	H_b (EA)	ΔE(del)[b] lp-σ^*	CT	k^a (XE)	n (XE)	k^a (EA)	n (EA)	3c−4e %	ω^a (EA)	ω_μ(% ω^a)
F(H)E···AR$_n$																
1	F(H)S···OH$_2$ (C_s)	1.641	2.646	5.2	5.1	0.144	0.012	9.4	0.035	4.122	0.944	0.185	0.123	13	172	136 (2;9.4), 163 (3;90.5)
2	F(H)Se···OH$_2$ (C_s)	1.779	2.615	7.0	6.5	0.166	0.010	14.8	0.048	3.611	0.866	0.216	0.136	16	166	159 (3;99.7)
3	F(H)Te···OH$_2$ (C_s)	1.947	2.695	8.3	7.7	0.173	0.004	16.5	0.045	3.376	0.828	0.252	0.151	18	173	165 (3;99.9)
4	F(H)S···SH$_2$ (C_s)	1.642	3.074	4.1	4.0	0.120	0.003	11.4	0.054	3.964	0.920	0.125	0.095	10	106	104 (2;100.0)
5	F(H)Se···SH$_2$ (C_s)	1.784	2.998	6.1	5.5	0.158	−0.005	21.8	0.085	3.383	0.829	0.155	0.109	13	107	104 (2;100.0)
6	F(H)Te···SH$_2$ (C_s)	1.950	3.101	7.2	6.6	0.160	−0.009	24.0	0.091	3.212	0.802	0.161	0.112	14	103	98 (2;69.1), 105 (3;30.9)
7	F(H)S···SeH$_2$ (C_s)	1.644	3.138	4.0	3.9	0.158	−0.005	12.6	0.060	3.852	0.903	0.107	0.086	9	89	77 (2;100.0)
8	F(H)Se···SeH$_2$ (C_s)	1.787	3.087	6.2	5.7	0.155	−0.007	23.6	0.100	3.265	0.810	0.147	0.106	13	79	76 (2;100.0)
9	F(H)Te···SeH$_2$ (C_s)	1.953	3.192	7.5	6.9	0.157	−0.011	26.0	0.108	3.152	0.792	0.184	0.123	15	79	77 (2;99.9)
10	F(H)S···TeH$_2$ (C_s)	1.647	3.273	4.3	4.1	0.126	−0.002	15.1	0.078	3.648	0.872	0.093	0.078	9	79	67 (1;100.0)
11	F(H)Se···TeH$_2$ (C_s)	1.793	3.200	6.6	6.0	0.163	−0.010	28.5	0.128	3.060	0.777	0.144	0.104	13	70	67 (1;100.0)
12	F(H)Te···TeH$_2$ (C_s)	1.959	3.311	8.1	7.4	0.163	−0.013	32.1	0.141	2.980	0.763	0.169	0.116	15	66	64 (1;100.0)
13	F(H)S···FH (C_1)	1.629	2.828	2.3	2.5	0.086	0.012	3.3	0.010	4.411	0.987	0.048	0.051	5	82	59 (1;72.5), 94 (2;27.2)
14	F(H)Se···FH (C_1)	1.766	2.780	3.1	3.1	0.099	0.012	5.8	0.016	3.911	0.912	0.134	0.099	11	113	120 (3;98.9)
15	F(H)Te···FH (C_1)	1.934	2.864	3.8	3.6	0.104	0.009	6.8	0.018	3.584	0.862	0.143	0.104	12	121	119 (3;99.5)
16	F(H)S···NH$_3$ (C_s)	1.663	2.518	8.1	7.6	0.238	−0.014	23.9	0.092	3.315	0.818	0.183	0.122	15	177	159 (2;100.0)
17	F(H)Se···NH$_3$ (C_s)	1.806	2.501	11.7	10.6	0.267	−0.027	34.6	0.114	2.999	0.766	0.287	0.164	21	202	186 (4;100.0)
18	F(H)Te···NH$_3$ (C_s)	1.968	2.616	13.9	12.9	0.254	−0.029	33.7	0.111	2.960	0.760	0.382	0.198	26	226	207 (4;100.0)
F(H)E···AR$_n$																
19	F(H)S···FCH$_3$ (C_1)	1.633	2.747	3.0	3.6	0.125	0.009	3.6	0.011	4.365	0.981	0.112	0.088	9	126	79 (3;1.5) 104 (4;3.4), 116 (5;94.3)
20	F(H)Se···FCH$_3$ (C_1)	1.769	2.706	4.0	4.4	0.114	0.013	6.4	0.018	3.856	0.904	0.140	0.102	11	124	83 (3;6.0) 113 (5;88.9), 113 (6;4.1)
21	F(H)Te···FCH$_3$ (C_1)	1.937	2.769	5.0	5.1	0.125	0.009	8.2	0.022	3.529	0.853	0.137	0.101	12	118	87(3;39.7), 117 (5;56.4), 162 (6;3.6)
22	F(H)S···O(CH$_3$)$_2$ (C_s)	1.646	2.540	6.6	7.2	0.185	0.007	9.3	0.040	3.937	0.916	0.202	0.130	14	179	68 (1;1.1), 136 (4;98.3)
23	F(H)Se···O(CH$_3$)$_2$ (C_s)	1.785	2.527	8.8	9.0	0.207	0.002	15.2	0.052	3.463	0.842	0.263	0.155	18	183	129 (4;85.6), 147 (5;13.2)
24	F(H)Te···O(CH$_3$)$_2$ (C_1)	1.951	2.620	10.4	10.5	0.204	−0.003	16.0	0.052	3.263	0.810	0.308	0.172	21	192	114 (4;2.6), 133 (5;97.0)
25	F(H)S···N(CH$_3$)$_3$ (C_s)	1.691	2.306	12.3	13.2	0.397	−0.088	36.8	0.141	2.648	0.706	0.329	0.179	25	240	147 (4;98.3), 433 (10;1.6)
26	F(H)Se···N(CH$_3$)$_3$ (C_s)	1.822	2.391	15.8	16.5	0.360	−0.074	40.1	0.133	2.701	0.715	0.442	0.218	30	251	142 (4;97.8), 445 (12;2.2)
27	F(H)Te···N(CH$_3$)$_3$ (C_s)	1.976	2.545	17.9	18.9	0.313	−0.058	34.4	0.114	2.776	0.728	0.465	0.225	31	250	137 (3;97.9), 450 (12;2.1)
28	F(H)S···P(CH$_3$)$_3$ (C_s)	1.792	2.316	13.4	11.3	0.633	−0.244	198.9	0.415	1.194	0.418	0.489	0.233	56	230	154 (4;92.9), 322 (11;6.6)
29	F(H)Se···P(CH$_3$)$_3$ (C_s)	1.887	2.497	17.4	15.3	0.385	−0.113	115.5	0.329	1.711	0.530	0.502	0.237	45	195	126 (4;96.2), 311 (12;3.8)
30	F(H)Te···P(CH$_3$)$_3$ (C_s)	2.016	2.714	19.4	17.8	0.385	−0.113	87.9	0.259	2.129	0.612	0.524	0.244	40	189	118 (4;96.5) 308 (12;3.4)
31	F(H)S···As(CH$_3$)$_3$ (C_s)	1.696	2.686	7.9	7.5	0.319	−0.058	43.0	0.216	1.772	0.542	0.131	0.098	18	100	78 (4;99.9)
32	F(H)Se···As(CH$_3$)$_3$ (C_s)	1.843	2.717	12.1	11.2	0.333	−0.068	59.9	0.249	2.059	0.599	0.290	0.165	28	113	204 (3;100.0)
33	F(H)Te···As(CH$_3$)$_3$ (C_s)	1.994	2.882	14.2	13.6	0.288	−0.059	53.9	0.224	2.331	0.649	0.359	0.190	29	113	90 (4;99.5)
X(H)E···NH$_3$																
34	F$_3$C(H)Se···NH$_3$ (C_s)	1.964	3.029	4.3	4.1	0.097	0.010	6.8	0.025	2.573	0.693	0.119	0.092	13	130	118 (4;99.8)
35	F$_3$C(H)Te···NH$_3$ (C_s)	2.187	2.987	6.2	5.6	0.126	0.005	11.4	0.044	2.048	0.597	0.121	0.093	16	127	116 (4;100.0)
36	F$_2$N(H)S···NH$_3$ (C_s)	1.759	2.862	5.1	5.1	0.116	0.010	7.2	0.032	2.536	0.686	0.124	0.095	14	147	82 (3;10.0), 134 (4;90.0)
37	F$_2$N(H)Se···NH$_3$ (C_s)	1.931	2.763	7.2	6.4	0.163	0.004	16.3	0.061	2.064	0.600	0.166	0.115	19	154	140 (5;99.8)
38	F$_2$N(H)Te···NH$_3$ (C_1)	2.154	2.758	9.8	8.7	0.197	−0.010	23.3	0.088	1.723	0.532	0.218	0.137	26	171	145 (4;1.4), 157 (5;98.6)
39	FO(H)S···NH$_3$ (C_1)	1.617	2.784	6.2	6.1	0.141	0.008	9.3	0.041	2.884	0.747	0.145	0.105	14	159	125 (3;47.9), 149 (4;52.0)

J. Phys. Chem. A 2017, 121, 6845−6862 DOI: 10.1021/acs.jpca.7b06479

Table 2. continued

#	complexes (sym.)	r (XE)	r (EA)	ΔE DFT	ΔE CCSD(T)	ρ_b (EA)	H_b (EA)	ΔE(del)[b] lp-σ^*	CT	k^a (XE)	n (XE)	k^a (EA)	n (EA)	3c–4e %	ω^a (EA)	ω_μ(% ω^a)
X(H)E···NH$_3$																
40	FO(H)Se···NH$_3$ (C_1)	1.807	2.664	9.0	8.1	0.190	−0.001	20.0	0.074	2.478	0.676	0.212	0.134	20	174	159 (4;99.9)
41	FO(H)Te···NH$_3$ (C_1)	2.013	2.695	11.7	10.6	0.218	−0.016	26.3	0.096	2.308	0.645	0.291	0.166	26	198	181 (4;100.0)
F(Y)E···NH$_3$																
42	F(CH$_3$)S···NH$_3$ (C_s)	1.648	2.917	4.3	4.4	0.101	0.011	5.6	0.022	3.780	0.892	0.062	0.060	7	104	90 (2;99.8)
43	F(CH$_3$)Se···NH$_3$ *anti* (C_s)	1.804	2.624	7.9	7.2	0.207	−0.006	23.4	0.079	2.989	0.765	0.184	0.123	16	162	128 (3;15.4), 154 (5;84.6)
	F(CH$_3$)Se···NH$_3$ *syn* (C_s)	1.810	2.568	9.1	8.5	0.232	−0.014	26.9	0.094	2.910	0.751	0.244	0.147	20	186	171 (5;100.0)
44	F(CH$_3$)Te···NH$_3$ (C_s)	1.843	2.717	12.1	11.2	0.333	−0.068	59.9	0.249	2.059	0.599	0.290	0.165	28	113	204 (3;100.0)
45	F(CF$_2$H)S···NH$_3$ (C_s)	1.638	2.729	7.0	7.0	0.147	0.007	10.1	0.046	3.799	0.895	0.084	0.073	8	121	106 (3;100.0)
46	F(CF$_2$H)Se···NH$_3$ *anti* (C_s)	1.788	2.578	10.9	10.3	0.233	−0.014	26.0	0.092	3.274	0.812	0.242	0.147	18	186	161 (5;77.8), 185 (6;22.2)
	F(CF$_2$H)Se···NH$_3$ *syn* (C_s)	1.819	2.421	15.7	14.2	0.323	−0.052	40.7	0.142	2.784	0.730	0.414	0.209	29	243	212 (5;2.7), 225 (6;97.2)
47	F(CF$_2$H)Te···NH$_3$ (C_s)	1.955	2.650	13.8	13.1	0.240	−0.024	28.2	0.100	3.161	0.793	0.333	0.181	23	211	196 (6;99.5)
48	F(CF$_3$)Se···NH$_3$ *anti* (C_s)	1.801	2.458	11.5	11.0	0.302	−0.041	37.0	0.132	3.038	0.773	0.333	0.181	23	218	159 (3;13.8), 182 (5;2.7), 211 (6;83.4)
	F(CF$_3$)Se···NH$_3$ *syn* (C_s)	1.795	2.454	14.6	14.2	0.303	−0.042	36.0	0.133	3.142	0.790	0.376	0.196	25	231	209 (5;87.8), 217 (6;12.1)
49	F$_2$S···NH$_3$ (C_s)	1.629	2.572	6.7	6.3	0.221	−0.008	15.8	0.072	3.795	0.895	0.156	0.110	12	165	129 (2;18.8), 152 (4;81.2)
50	F$_2$Se···NH$_3$ (C_s)	1.775	2.477	11.7	10.7	0.289	−0.036	28.2	0.109	3.343	0.823	0.297	0.168	20	206	190 (4;99.1)
51	F$_2$Te···NH$_3$ (C_s)	1.943	2.560	15.5	14.6	0.292	−0.046	27.5	0.118	3.251	0.808	0.376	0.196	24	225	207 (4;98.2)
52	F(CN)S···NH$_3$ (C_s)	1.653	2.465	10.8	10.4	0.275	−0.026	26.3	0.127	3.372	0.828	0.220	0.138	17	196	175 (3;99.9)
53	F(CN)Se···NH$_3$ (C_s)	1.792	2.465	15.1	14.1	0.298	−0.040	37.2	0.143	3.177	0.796	0.366	0.192	24	228	210 (5;100.0)
54	F(CN)Te···NH$_3$ (C_s)	1.953	2.572	17.9	17.0	0.286	−0.044	36.9	0.137	3.178	0.796	0.400	0.204	26	232	213 (5;100.0)
X=E···NH$_3$																
55	F$_2$CS···NH$_3$ (C_s)	1.595	3.381	1.0	1.5	0.045	0.009	1.5	0.006	6.702	1.300	0.034	0.040	3	77	64 (4;100.0)
56	F$_2$CSe···NH$_3$ (C_s)	1.749	3.198	2.5	2.5	0.072	0.009	4.2	0.028	5.004	1.073	0.062	0.060	6	94	84 (4;100.0)
57	F$_2$CTe···NH$_3$ (C_s)	1.984	3.148	4.3	3.9	0.096	0.008	7.7	0.014	3.395	0.831	0.131	0.098	12	133	121 (4;100.0)
58	OCS···NH$_3$ (C_{3v})	1.566	3.273	1.7	2.0	0.054	0.010	2.1	0.008	7.248	1.368	0.047	0.050	4	90	77 (3;100.0)
59	OCSe···NH$_3$ (C_{3v})	1.721	3.091	3.5	3.3	0.085	0.010	5.9	0.019	5.037	1.077	0.105	0.085	8	122	111 (3;100.0)
60	OCTe···NH$_3$ (C_{3v})	1.967	3.033	5.7	5.0	0.116	0.007	11.1	0.040	2.836	0.739	0.131	0.098	13	133	122 (3;100.0)
61	FNS···NH$_3$ (C_1)	1.534	2.659	5.5	4.4	0.192	0.000	**11.3**	0.084	7.073	1.346	0.137	0.101	7	155	69 (2;1.1) 143 (3;97.7), 185 (4;1.3)
62	FNSe···NH$_3$ (C_1)	1.690	2.649	7.0	5.3	0.213	−0.005	**26.1**	0.099	5.656	1.163	0.169	0.116	10	155	145 (3;99.3)
63	FNTe···NH$_3$ (C_1)	1.905	2.661	9.2	6.6	0.248	−0.026	**37.7**	0.124	4.326	0.975	0.219	0.137	14	172	160 (3;99.5)
FH$_2$E$^+$···NH$_3$																
64	F(H$_2$)S$^+$···NH$_3$ (C_s)	1.614	2.188	38.7	36.9	0.528	−0.173	57.8	0.249	4.008	0.927	0.674	0.287	31	343	308 (4;99.9)
65	F(H$_2$)Se$^+$···NH$_3$ (C_1)	1.748	2.308	39.2	37.5	0.439	−0.123	59.0	0.218	3.921	0.914	0.718	0.300	33	320	294 (4;100.0)
66	F(H$_2$)Te$^+$···NH$_3$ (C_1)	1.906	2.451	38.9	37.6	0.382	−0.096	51.1	0.190	3.833	0.900	0.739	0.305	34	315	290 (4;100.0)
67	H$_3$S$^+$···NH$_3$ (C_s)	1.362	2.730	19.1	18.4	0.171	0.002	9.9	0.053	3.803	0.896	0.291	0.166	18	225	208 (2;100.0)
68	FH(CN)S$^+$···NH$_3$ (C_s)	1.607	2.189	39.1	37.8	0.542	−0.178	57.8	0.279	4.035	0.931	0.658	0.283	30	339	300 (5;17.7), 305 (6;82.0)
X(Y)E···Cl$^-$																
69	F$_3$C(H)Se···Cl$^-$ (C_s)	1.986	2.892	17.0	17.4	0.183	−0.006	24.9	0.118	2.105	0.607	0.244	0.147	24	131	130 (3;99.0)
70	F$_2$N(H)Se···Cl$^-$ (C_s)	2.015	2.639	25.9	25.8	0.308	−0.050	59.6	0.247	1.253	0.432	0.412	0.208	48	170	170 (4;99.8)
71	FO(H)Se···Cl$^-$ (C_s)	1.880	2.623	28.4	28.2	0.315	−0.054	58.5	0.250	1.206	0.421	0.437	0.216	51	175	175 (3;99.9)
72	F(H)S···Cl$^-$ (C_s)	1.786	2.479	22.5	22.5	0.389	−0.086	74.6	0.308	1.432	0.472	0.397	0.203	43	201	195 (1;100.0)
73	F(H)Se···Cl$^-$ (C_s)	1.920	2.538	30.2	29.4	0.371	−0.084	85.3	0.306	1.595	0.506	0.587	0.263	52	173	202 (3;100.0)

DOI: 10.1021/acs.jpca.7b06479
J. Phys. Chem. A 2017, 121, 6845−6862

Table 2. continued

#	complexes (sym.)	r (XE)	r (EA)	ΔE DFT	ΔE CCSD(T)	ρ_b (EA)	H_b (EA)	ΔE(del)[b] lp-σ^*	CT	k^a (XE)	n (XE)	k^a (EA)	n (EA)	3c−4e %	ω^a (EA)	ω_μ(% ω^a)
X(Y)E···Cl⁻																
74	F(H)Te···Cl⁻ (C_s)	2.068	2.656	36.6	36.1	0.349	−0.083	78.6	0.287	1.807	0.549	0.718	0.300	55	202	210 (3;100.0)
75	F(CF_2H)S···Cl⁻ (C_s)	1.741	2.546	27.3	29.0	0.346	−0.063	57.3	0.277	1.814	0.551	0.311	0.173	31	178	167 (2;99.1)
76	F(CF_2H)Se···Cl⁻ *anti* (C_s)	1.886	2.560	36.1	36.9	0.359	−0.076	72.6	0.294	1.881	0.564	0.538	0.248	44	194	196 (5;98.8)
	F(CF_2H)Se···Cl⁻ *syn* (C_s)	1.952	2.455	34.8	35.0	0.449	−0.129	108.1	0.372	1.373	0.459	0.772	0.314	69	232	232 (5;99.6)
77	F(CF_2H)Te···Cl⁻ (C_s)	2.043	2.661	43.5	44.2	0.348	−0.082	68.8	0.286	1.996	0.587	0.699	0.294	50	207	209 (5;99.9)
78	F(CN)S···Cl⁻ (C_s)	1.785	2.393	33.1	33.6	0.485	−0.135	94.9	0.410	1.571	0.501	0.647	0.280	56	256	249 (4;99.6)
79	F(CN)Se···Cl⁻ (C_s)	1.906	2.474	41.3	40.9	0.439	−0.121	102.5	0.376	1.779	0.544	0.792	0.320	59	235	235 (4;100.0)
80	F(CN)Te···Cl⁻ (C_s)	2.047	2.597	47.7	47.5	0.399	−0.111	90.1	0.339	1.973	0.582	0.903	0.348	60	236	237 (4;100.0)
X=E···Cl⁻																
81	F_2CS···Cl⁻ (C_s)	1.582	2.997	6.0	7.3	0.144	0.004	**15.1**	0.094	6.874	1.321	0.126	0.096	7	113	112 (3;99.1)
82	F_2CSe···Cl⁻ (C_s)	1.745	2.962	9.9	10.9	0.164	0.000	**15.0**	0.113	4.509	1.002	0.183	0.122	12	113	28 (1;3.9), 120 (3;96.2)
83	F_2CTe···Cl⁻ (C_s)	2.005	2.935	16.2	17.7	0.203	−0.015	**19.2**	0.152	2.503	0.681	0.215	0.136	20	115	19 (1;9.4), 131 (3;90.6)
84	OCS···Cl⁻ ($C_{\infty v}$)	1.564	3.127	8.0	9.1	0.106	0.008	7.0	0.042	7.071	1.346	0.134	0.099	7	117	102 (3;100.0)
85	OCSe···Cl⁻ ($C_{\infty v}$)	1.730	2.987	13.2	13.3	0.150	0.002	16.5	0.083	4.409	0.987	0.200	0.129	13	118	115 (3;100.0)
86	OCTe···Cl⁻ ($C_{\infty v}$)	2.009	2.893	20.2	20.5	0.218	−0.021	35.1	0.159	1.955	0.579	0.338	0.183	32	144	144 (3;100.0)
87	FNS···Cl⁻ (C_1)	1.535	2.431	26.7	25.8	0.452	−0.107	**74.0**	0.376	5.992	1.207	0.507	0.238	20	227	113 (1;8.1), 227 (2;88.8), 314 (3;3.1)
88	FNSe···Cl⁻ (C_1)	1.702	2.509	30.0	28.2	0.410	−0.095	**56.8**	0.361	4.911	1.060	0.576	0.259	24	201	97 (1;1.7), 205 (2;98.0)
89	FNTe···Cl⁻ (C_1)	1.923	2.595	36.8	33.9	0.401	−0.107	**116.6**	0.361	3.814	0.897	0.740	0.306	34	213	240 (3;94.9)
homodimers																
90	$(F(H)Se)_2$ (C_i)	1.786	2.665	7.7	6.4	0.301	−0.047	37.9	0.000	2.512	0.682	0.252	0.151	22	104	92 (2;99.9)
91	$(F(H)Te)_2$ (C_i)	1.956	2.943	11.0	10.1	0.318	−0.074	44.4	0.000	2.519	0.683	0.405	0.206	30	103	92 (2;99.4)
92	$(FNSe)_2$ (C_i)	1.691	3.686	2.7	2.9	0.060	0.002	1.2	0.000	5.674	1.165	0.027	0.035	3	34	28 (3;83.0), 41 (4;17.0)
93	$(FNTe)_2$ (C_i)	1.928	2.828	8.5	7.9	0.413	−0.123	67.9	0.000	3.631	0.869	0.391	0.201	23	101	54 (3;17.2), 113 (4;82.8)
94	$((Me_2N)_2Se)_2$ (C_{2h})	1.832	3.216	4.7		0.073	0.007	2.6	0.000	2.846	0.740	0.075	0.068	9	104	37 (3;27.2), 49 (5;70.7)
95	$((Me_2N)_2Te)_2$ (C_{2h})	2.011	3.005	9.8		0.130	0.002	8.1	0.000	2.662	0.709	0.081	0.071	10	104	44 (3;96.7), 52 (5;2.8)
96	$(F(PMe_2)Te)_2$ (C_{2h})	2.061	2.670	28.0		0.429	−0.139	86.4	0.000	1.657	0.519	0.690	0.292	56	216	103 (4;57.1), 117 (5;34.3), 296 (19;2.5)
97	$(H_2C_2N_2Se)_2$ (C_{2h})	1.787	2.994	6.0	6.3	0.095	0.011	3.6	0.000	3.331	0.821	0.121	0.093	11	131	58 (3;43.2), 73 (4;56.8)
98	$(H_2C_2N_2Te)_2$ (C_{2h})	2.004	2.707	13.5	13.6	0.210	−0.013	11.8	0.000	2.471	0.675	0.180	0.121	18	155	69 (2;81.3), 80 (4;18.6)
99	$(F_2C_2N_2Te)_2$ (C_{2h})	2.022	2.685	15.3		0.213	−0.013	13.4	0.000	2.378	0.658	0.241	0.146	22	180	58 (3;19.2), 69 (4;80.6)
100	$(Me_2C_2N_2Te)_2$ (C_{2h})	2.015	2.695	13.8		0.216	−0.015	12.6	0.000	2.569	0.692	0.210	0.134	19	168	58 (3;13.6), 65 (4;86.3)

[a]Computed at ωB97X-D/aug-cc-pVTZ(-PP for Se, As, and Te). Bond distances r(XE) and r(EA) in Å; binding energy ΔE(DFT) and CCSD(T)/aug-cc-pVTZ(-PP)//ωB97X-D ΔE in kcal/mol, where the latter was used to estimate ωB97X-D reliability. Density at EA critical point ρ_b in e/Å^3; energy density at EA critical point H_b in Hartree/Å^3; lp(A) → σ^*(XE) delocalization energy ΔE(del) in kcal/mol; NPA charge transfer in e, local XE and EA stretching force constants in mdyn/Å, EA local stretching frequency ω^a in cm^{-1}, 3c−4e % character calculated from n(EA)/n(XE), and normal-mode frequencies related to EA stretching ω_μ in cm^{-1}, their mode order no., and % local stretching character (ω^a %) . [b]ΔE(del) values for lp → π^* are given in bold.

DOI: 10.1021/acs.jpca.7b06479
J. Phys. Chem. A 2017, 121, 6845−6862

molecular orbital (HOMO) of the Ch acceptors is the lp(A) orbital, and the lowest unoccupied molecular orbital orbital (LUMO) of the Ch donors is the σ^*(EX) for divalent chalcogens and π^*(EX) for double bonded chalcogens. Orbital energies calculated at the HF/6-31g(d) level were used to measure the electron donor ability of the Ch acceptors (Figure S1) and electron acceptor ability of the Ch donors (Figure S2), where a HOMO of higher energy or a LUMO of lower energy results in a smaller HOMO−LUMO energy gap ($\Delta\epsilon$) and therefore, in a stronger CT. Because of the basis set dependence of orbital energies, vertical ionization potentials calculated at CCSD(T)aug-cc-pVTZ(-PP)//ωB97X-D were used to compare the electron donor ability of Ch acceptors of different periods.

The electrostatic attractive capabilities of the monomers were accessed by investigating the electrostatic potential $V(\mathbf{r})$ mapped on the 0.001 e/Bohr^3 electron density surface of the monomers (Figures S3 and S4). Where the maximum $V(\mathbf{r})$ at the σ−*hole* region of Ch donors (V_{max}) and the minimum $V(\mathbf{r})$ at the lp(A) region of the Ch acceptors provide a measure for the electrostatic attraction (Table 3 and 4).

Table 3. Summary of Chalcogen Acceptor Properties[a]

acceptors	IP(CCSD(T))	NBO(A)	$V(r)_{min}$	α_{iso}
HF	16.2	−0.554	−0.90	5.6
OH_2	12.7	−0.929	−1.43	9.7
SH_2	10.4	−0.281	−0.74	24.7
SeH_2	9.8	−0.172	−0.67	31.7
TeH_2	9.0	0.038	−0.57	44.2
NH_3	10.9	−1.056	−1.63	14.3
PH_3	10.5	0.025	−0.73	30.8
AsH_3	10.5	0.114	−0.46	36.0
FMe	13.4	−0.380	−0.98	17.1
OMe_2	10.2	−0.559	−1.34	33.6
NMe_3	8.5	−0.512	−1.34	50.8
PMe_3	8.6	0.761	−1.25	67.6
$AsMe_3$	8.7	0.801	−0.95	73.2
$H_2C_2N_2Se$	9.7	−0.618	−1.17	60.2
$H_2C_2N_2Te$	10.2	−0.678	−1.24	73.6
$F_2C_2N_2Te$	9.3	−0.710	−0.99	72.9
$Me_2C_2N_2Te$	8.4	−0.698	−1.30	101.3
F^-	3.3	−1.000	−7.31	9.0
Cl^-	3.5	−1.000	−6.05	29.0

[a]Vertical ionization potential computed at ωB97X-D/aug-cc-pVTZ (PP for Se As and Te) geometry and with CCSD(T) /aug-cc-pVTZ(-PP) energies (without including the zero point energy) in eV. NBO charges at the Ch acceptor heteroatom A, minimum electrostatic potential at the lone pair region of A (V_{min}) in kcal/mol, isotropic polarizability in Bohr^3, and total dipole moment in Debye.

It is well-known that other contributions such as dispersion and exchange-repulsion can also play an important role for the stability of ChB complexes.[38,39,67] These contributions will be explicitly discussed only when they are required to explain qualitative changes in the ChB strength order. A SAPT0 energy decomposition was used[132−134] for this purpose.

The calculation of the local mode properties was performed with the program COLOGNE2016.[135] CCSD(T) energies were obtained with the package CFOUR.[136] For the NBO analysis, the program NBO 6[131] was used. The local properties of the electron density distribution $\rho(\mathbf{r})$ and energy density distribution $H(\mathbf{r})$ at the ChB critical point $\mathbf{r}_b$ and the electrostatic potentials were analyzed with the program Multiwfn.[137] The SAPT0 energy decomposition[132] was carried out with Molpro[138] and DFT calculations were performed with Gaussian09.[139]

3. RESULTS AND DISCUSSION

Figure 2 contains a schematic representation of complexes **1**−**100**. They are separated into four groups (I−IV). Group I (**1**−**33**) provides a systematic investigation of the effect of varying the Ch acceptor AR_n. Group II is used to study the effect of different substituents at the chalcogen (**34**−**63**). Group III (**64**−**89**) contains charge assisted ChB complexes, whereas group IV (**90**−**100**) is used to investigate ChB in symmetric homodimer complexes.

The data for all ChB complexes are summarized in Table 2, which contains bond lengths $r(XE)$ and $r(EA)$ in Å, binding energies (ΔE(DFT) and ΔE(CCSD(T)) in kcal/mol, the electron density ρ_b(EA) in electron/Å^3, and the energy density H_b(EA) in hartree/Å^3 at the ChB density critical point ($\mathbf{r}$), NBO delocalization energies $\Delta E(del)$ in kcal/mol, intermonomer CT obtained from the natural population analysis (NPA partial atomic charges[140]) in electrons, local stretching force constants $k^a(XE)$ and $k^a(EA)$ in mdyn/Å, BSO values $n(XE)$ and $n(EA)$, degree of 3c−4e bonding in %, and the frequency of that normal mode, which has dominant XB stretching character. The latter is given to provide vibrational spectroscopist information where the ChB stretching band should be found when recording either infrared or Raman spectra.

Tables 3 and 4 provide a summary of the Ch acceptors (Tables 3) and the Ch donors (Tables 4) properties. Including vertical ionization energies of Ch acceptors in eV, NPA partial atomic charges of A and E atoms, electrostatic potentials V_{min} and V_{max} in eV, isotropic polarizabilities α_{iso} in Bohr^3, $r(XE)$ in Å, $k^a(XE)$ in mdyn/Å, and $n(XE)$.

Figure 3 provides an ordering of all ChBs investigated according to their intrinsic bond strength given by the BSO values. ChBs vary from weak interactions ($n(EA) < 0.1$) to normal ($0.1 \le n(EA) \le 0.2$) and to strong interactions ($n(EA) > 0.2$), where the latter are mostly charge assisted ChBs.

The relationship between the strength and the nature of the ChBs is shown on Figure 4. As the ChB varies from weak to strong bonds, H_b changes from slightly positive (electrostatic) to negative (covalent), indicating that an increase in the strength of the ChB tend to be accompanied by an increase in its covalent character, given by a more negative H_b according to Cremer−Kraka criteria.[126] A comparison of the $n(EA)$ values of complexes where E = S, Se and Te (Table 2) confirme that the ChB becomes stronger with the increase in the polarizability of the chalcogen atom (S < Se < Te) for the entire set (a similar trend is not always found for XB[97,98]).

In the following section, rather than discussing each complex individually, we describe the most important electronic effects present in each group (I−IV), which are responsible for the ChB strength trends shown in the $k^a(EA)$ *vs* $n(EA)$ power relationship diagrams. Some representative complexes, and complexes that deviate from the expected trends are discussed individually.

ChB Strength Dependence on the Ch Acceptors. The ChB strength ordering of the chalcogen-chalcogen interactions in F(H)E···E′H_2 (complexes **1**−**12**), shown on Figure 5a can be rationalized by considering two major electronic effects with opposing impact on the ChB strength. (i) Descending within

DOI: 10.1021/acs.jpca.7b06479
J. Phys. Chem. A 2017, 121, 6845−6862

Table 4. Summary of Chalcogen Donor Properties[a]

Ch donors	r(XE)	k^a(XE)	n(XE)	NBO(E)	$V(r)_{max}$	α_{iso}
$F_3C(H)Se$	1.961	2.598	0.697	0.051	1.29	44.7
$F_3C(H)Te$	2.176	2.144	0.615	0.235	1.50	57.3
$F_2N(H)S$	1.754	2.635	0.704	0.183	1.56	36.6
$F_2N(H)Se$	1.914	2.215	0.628	0.274	1.69	43.8
$F_2N(H)Te$	2.124	1.839	0.556	0.456	1.90	56.5
FO(H)S	1.606	3.386	0.830	0.437	1.81	32.5
FO(H)Se	1.774	3.144	0.790	0.486	2.02	38.2
FO(H)Te	1.971	2.811	0.734	0.653	2.25	49.4
F(H)S	1.626	4.605	1.016	0.393	1.75	24.0
F(H)Se	1.759	3.993	0.925	0.503	2.14	30.2
F(H)Te	1.926	3.652	0.872	0.691	2.40	41.4
$F(CH_3)S$	1.633	4.404	0.986	0.586	1.25	36.2
$F(CH_3)Se(anti)$	1.766	3.795	0.895	0.687	1.74	42.7
$F(CH_3)Se(syn)$	1.768	3.872	0.906	0.677	1.81	42.6
$F(CH_3)Te$	1.935	3.544	0.855	0.854	2.13	54.3
$F(CF_2H)S$	1.616	4.747	1.036	0.588	1.98	37.5
$F(CF_2H)Se(anti)$	1.751	4.128	0.945	0.671	2.43	44.0
$F(CF_2H)Se(syn)$	1.760	4.036	0.931	0.665	2.75	43.9
$F(CF_2H)Te$	1.920	3.711	0.881	0.831	2.71	55.6
$F(CF_3)Se(anti)$	1.750	4.221	0.959	0.673	1.94	44.2
$F(CF_3)Se(syn)$	1.747	4.265	0.966	1.066	2.49	44.4
F_2S	1.600	4.922	1.061	0.937	1.58	23.7
F_2Se	1.734	4.378	0.983	1.053	2.11	29.2
F_2Te	1.905	3.821	0.899	1.223	2.42	39.0
F(CN)S	1.614	4.636	1.020	0.735	1.95	37.8
F(CN)Se	1.746	4.141	0.947	0.849	2.44	43.4
F(CN)Te	1.912	3.767	0.890	1.036	2.72	53.8
F_2CS	1.595	6.736	1.304	−0.028	0.51	35.5
F_2CSe	1.743	5.316	1.116	0.017	0.87	43.3
F_2CTe	1.967	3.837	0.901	0.098	1.15	58.1
OCS	1.564	7.514	1.401	0.003	0.82	34.1
OCSe	1.711	5.545	1.148	0.041	1.21	41.8
OCTe	1.938	3.973	0.922	0.103	1.48	56.4
FNS	1.540	7.168	1.358	0.406	1.23	31.2
FNSe	1.694	5.601	1.155	0.452	1.40	38.1
FNTe	1.909	4.472	0.996	0.551	1.50	51.1
$H_2C_2N_2Se$	1.788	3.261	0.810	0.885	1.08	60.2
$H_2C_2N_2Te$	1.993	2.631	0.703	1.004	1.30	73.6
$F_2C_2N_2Te$	2.002	2.733	0.721	1.042	1.87	72.9
$Me_2C_2N_2Te$	1.994	2.715	0.718	0.976	1.09	101.3
H_3S^+	1.356	3.973	0.922	0.292	7.29	17.7
FH_2S^+	1.553	5.819	1.184	1.021	8.66	18.5
FH_2Se^+	1.692	5.387	1.126	1.200	8.66	23.2
FH_2Te^+	1.861	4.806	1.045	1.538	8.53	31.0
$FH(CN)S^+$	1.551	5.610	1.156	1.250	8.28	32.9

[a]Computed at ωB97X-D/aug-cc-pVTZ (PP for Se As and Te). Bond distances r(XE) in Å, local YX stretching force constant k^a(XE) in mdyn/Å, and bond strength order n. NBO charges at E, maximum electrostatic potential at the σ-hole of E (V_{max}) in kcal/mol, isotropic polarizability in Bohr^3, and total dipole moment in Debye.

group XVI of the PT from A = O, S, Se, Te for AH_2 Ch acceptors, the lp(A) orbitals at AH_2 become increasingly diffuse, due to the higher number of occupied electron shells, leading to a decrease in the magnitude of the electrostatic potential (V_{min} = −1.43 (OH_2) ≪ −0.74 (SH_2) < −0.67 (SeH_2) < −0.57 (TeH_2) eV). (ii) Another consequence of the higher number of occupied electron shells is the decrease in the electronegativity of A atom (Pauling scale: χ = 3.44 (O); 2.58 (S); 2.55 (Se); 2.10 (Te)) resulting in lp(A) orbitals, which are higher in energy (lower IP, Table 3, thus decreased $\Delta\epsilon(2e)$) allowing a stronger CT (e.g., $\Delta E(del)$ = 32.1 (**12**) compared to 16.5 (**3**) kcal/mol). Complexes formed with OH_2 Ch acceptor (**1**−**3**) have the strongest ChBs among complexes **1**−**12** ($n(EA)$ = 0.123 (**1**), 0.136 (**2**), 0.151 (**3**) and ΔE = 5.1 (**1**), 6.5 (**2**), 7.7 (**3**) kcal/mol), indicating that the decrease in the magnitude of V_{min} descending within a period has a stronger effect on the bond strength over the increase of CT.

A decrease in the electronegativity of the Ch acceptor atom (A) does not necessarily weaken the electrostatic contributions. Figure 5a shows the strength ordering of ChB involving FHE (E = S, Se and Te) Ch donors and Ch acceptors across the second period of the PT (HF, OH_2, NH_3). There is an increase

DOI: 10.1021/acs.jpca.7b06479
J. Phys. Chem. A 2017, 121, 6845−6862

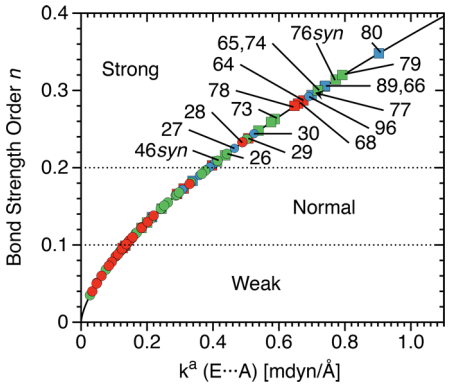

Figure 3. Power relationship between the relative bond strength order (BSO) n and the local stretching force constants k^a of complexes **1**−**100**. S···A ChB are shown in red, Se···A in green, and Te···A in blue for neutral complexes (circles) and charged complexes (squares) .

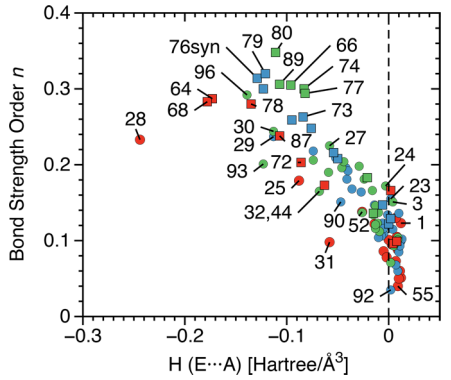

Figure 4. Comparison between the relative bond strength order (BSO) n and the energy density at the bond critical point H_b of the ChBs of complexes **1**−**100**. S···A ChB are shown in red, Se···A in green, and Te···A in blue for neutral complexes (circles) and charged complexes (squares) .

in the BSO from HF, to OH_2 and NH_3 (e.g., in this series the BSO for F(H)Te is $n(EA)$ = 0.104 (**15**), 0.151 (**3**), 0.198 (**18**)), which is supported by both an increase in CT (Table 2) and a lowering of V_{min} (−0.90 (HF); −1.43 (OH_2); −1.63 (NH_3 eV). The decrease in the electronegativity of A (Pauling scale: χ = 3.98 (F); 3.44 (O); 3.04 (N)) leads to a less contracted but still localized lp(A), which has a lower V_{min} (Table 3) and a higher lp(A) energy (Figure S1).

Methyl substituents at the Ch acceptor strengthen the ChB by increasing the polarizability of the Ch acceptor and by decreasing the lp(A) energy (which result in a decrease of $\Delta\epsilon(2e)$). In the case of the heteroatoms of third or higher periods, which are less electronegative than C (Pauling scale: χ(A) = 2.55 (C); 2.19 (P); 2.18 (As)), Me substituents withdraw charge from A (NPA partial atomic charge P = 0.761 e in PMe_3 and As = 0.801 e in $AsMe_3$), effectively contracting the density at lp(A). The more localized lp(A) forms a better overlap with σ^*(XE) and adopts a more negative electrostatic potential at lp(A) (V_{min} = −1.25 (PMe_3), −0.95 ($AsMe_3$) compared to −0.73 (PH_3), and −0.46 (AsH_3) eV).

A similar effect is also found for XB complexes.[75,97] and is responsible for the formation of complete 3c−4e bonds, inverse 3c−4e bonds and ion-pairs between dihalogens, interhalogens and phosphines. However, comparable ChB complexes have lower CT and 3c−4e character (with a maximum 3c−4e character of 56% (**28**) for the neutral complexes). The reduced CT and 3c−4e character in ChB is due to the lower electronegativity of the chalcogens, resulting in higher σ^*-orbital energies thus larger $\Delta\epsilon$(2e) and also due to the less effective lp(A)−σ^* overlap caused by the bent X-E-A geometry adopted by chalcogens to reduce the exchange-repulsion between lp(E) and lp(A) orbitals.

Figure 6 provides the ChB strength order for the complexes with methylated Ch acceptors (**19**−**33**). ChB complexes

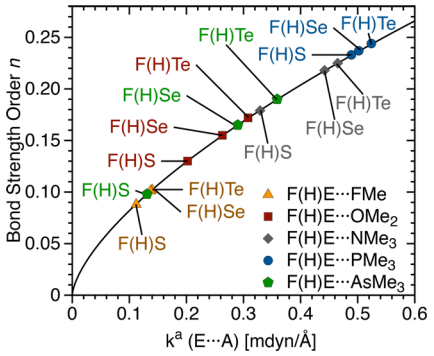

Figure 6. Power relationship between the relative bond strength order (BSO) n and the local stretching force constants k^a for complexes involving a series of methylated Ch acceptors.

involving methylated Ch acceptors of the second period (**19**−**27**) form stronger bonds (compared to OH_2 (**1**−**3**), FH

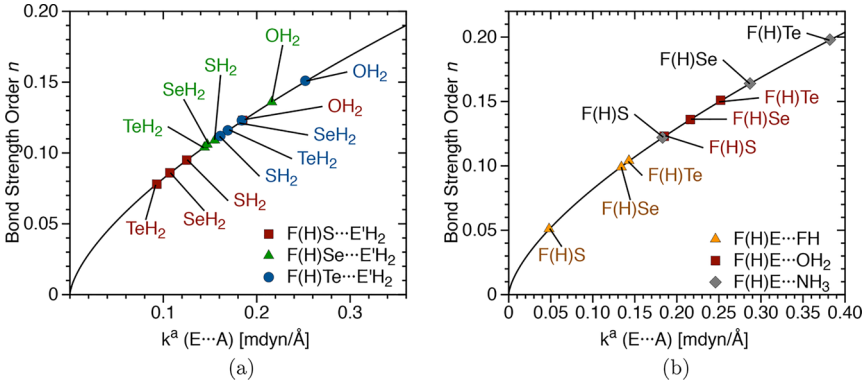

Figure 5. Power relationship between the relative bond strength order (BSO) n and the local stretching force constants k^a for (a) chalcogen−chalcogen interactions and (b) interactions between a chalcogen and a second period heteroatom.

DOI: 10.1021/acs.jpca.7b06479
J. Phys. Chem. A 2017, 121, 6845−6862

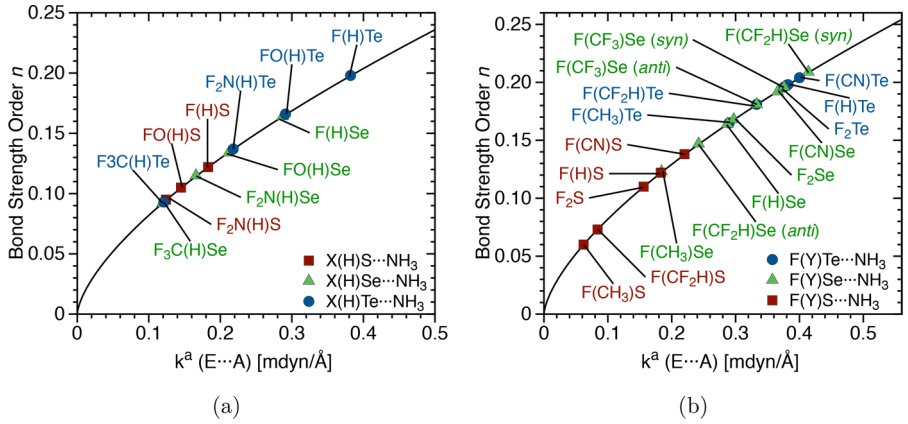

(a) (b)

Figure 7. Power relationship between the relative bond strength order (BSO) n and the local stretching force constants k^a for complexes involving NH_3: (a) with different subsituents (X) colinear to the ChB and (b) with different substituents at Y possition.

(**16**−**18**), and NH_3 (**16**−**18**) Ch acceptors) but the strength order with regard to the A is not altered (FMe < OMe_2 < NMe_3). The increase in strength occurs due to the increased CT in these complexes, which compensates the weaker electrostatic contribution (V_{min} = −1.34 NMe_3, −1.34 OMe_2 compared to −1.63 NH_3, and −1.43 OH_2). Descending within group XV of the PT (complexes **27**−**33**), there is an increase in the ChB strength (NMe_3 < PMe_3) followed by a decrease (PMe_3 > $AsMe_3$). The decrease is a result of the contracted (less diffuse) lp(P), which is more available than lp(N) (Figures S1 and S3), leading to a stronger CT (CT = 0.415 (**28**), 0.329 (**29**), 0.259 (**30**) compared to 0.141 (**25**), 0.133 (**26**), and 0.114 e (**27**)) and which has only a slightly higher electrostatic potential (V_{min} = −1.25 (PMe_3); −1.34 (NMe_3) eV), whereas the increase is a result of the increased diffuseness of lp(As) compared to lp(P), which decreases CT and increases V_{min} (−1.25 (PMe_3) −0.95 ($AsMe_3$) eV.

ChB Dependence on Ch Donors. Figure 7 shows the effect of different substituents at the X position (Figure 7a), and at the Y position, (Figure 7b), whereas Figure 8 shows the electron difference densities of selenium complexes for different Y substituents. The ChB bond becomes stronger when the most electronegative ligand (X) is arranged in a close to a collinear position to the ChB (in general X−E−A ≈ 170°; Figures S9−S12). A more electronegative substituent (X = F_3C < F_2N < FO < F) increases the CT by lowering the σ^*(XE) orbital energies (Figure S2, decreasing $\Delta\epsilon$(2e)), and by polarizing the chalcogen electron density leading to the formation of a more positive potential at the σ-hole region (V_{max} = 1.29 (F_3C(H)Se); 1.56 (F_2N(H)Se); 1.56 (FO(H)Se); 2.14 (F(H)Se) eV). The ligand Y, orthogonal to the ChB, plays a more subtle role, indirectly influencing the σ^*(XE) orbital energy (Figure S2), the magnitude of the σ-hole electrostatic potential (Figure S4), and also via exchange repulsion with lp(A).

For the Y substituent, the ChB strength increases in the series Y = CH_3 < CF_2H < F ≈ H < CF_3 < CN, where methyl substituents weaken the ChB by donating charge to the chalcogen (E), increasing the σ^*(XE) orbital energy (Figure S2) and decreasing V_{max} (Table 4). This can be reverted by substituting the hydrogens for fluorine atoms (Y = CF_2H and CF_3). By this, the group electronegativity increases, and the σ^*(XE) energy is lowered, enhancing charge transfer and strengthening the ChB. The CN group withdraws charge more effectively from the lone pairs of the chalcogen via lp(E) → π^* charge transfer increasing V_{max} (V_{max} = 2.44 eV in F(CN)Se compared to 2.14 eV in F(H)Se) and lowering the σ^*(XE) orbital energy (Figure S2). Although the Y = F substituent in F_2E withdraws charge from the chalcogen, it donates electron density back via lp(F) → σ^*(XE) ($\Delta E(del)$ = 14.3 kcal/mol), lowering V_{max} (V_{max} = 2.11 eV (F_2Se) compared to 2.14 eV (F(H)Se)).

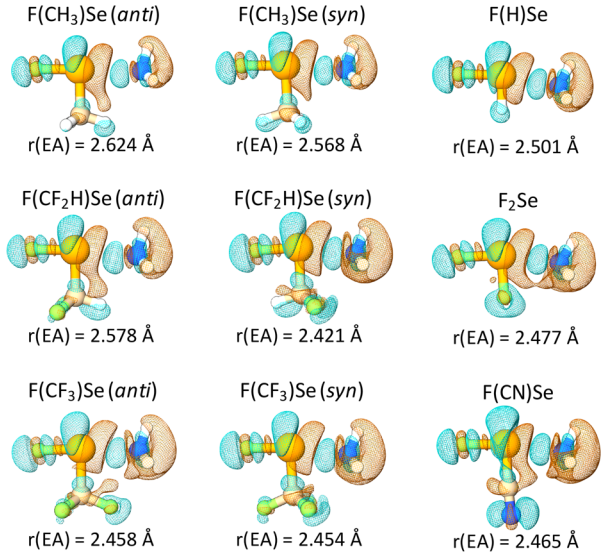

Figure 8. Electron difference density distributions $\Delta\rho(r)$ given for F(Y) Se···NH_3 complexes. $\Delta\rho(r)$ is plotted for an electron density surface of 0.001 au. Light blue regions indicate an increase in the electron density, and brown regions a density decrease relative to the superimposed density of the monomers. Calculated at ωB97X-D/aug-cc-pVTZ.

Exchange repulsion between lp(A) and Y weakens the ChB. This is evidenced in the electron difference densities of Figure 8 by a decrease of the electron density between Y and A (in brown) and by an electron density increase in the inferior extremity of Y (in light blue). If the Y group is rotated by 180° to the *syn* position, where the H (**43**, **46**) or F (**48**) atom at the molecular plane is not facing toward the Ch acceptor atom (A), the extension of the brown region decreases and the ChB becomes shorter and stronger ($n(EA)$ = 0.147 (**43** *syn*), 0.209 (**46** *syn*), 0.196 (**48** *syn*) compared to 0.123 (**43** *anti*), 0.147 (**46** *anti*), and 0.181(**48** *anti*)).

DOI: 10.1021/acs.jpca.7b06479
J. Phys. Chem. A 2017, 121, 6845−6862

The SAPT0 energy decomposition analysis (Table S4) confirms the important role of exchange repulsion for complex stabilization. By keeping the geometries of complexes **43**, **46**, and **48** frozen and rotating Y = CH_3, CF_2H, and CF_3 in F(Y)Se···NH_3 from the *anti* conformation to the *syn* position, the largest change in the interaction energy components occur for exchange repulsion, which decreases by 1.1 (**43**), 1.4 (**46**), and 2.4 (**48**) kcal/mol (see Supporting Information for other components).

ChB in sp² Hybridized Chalcogens. ChB involving sp^2-hybridized chalcogens represents a special case, where electrostatic and charge transfer contributions are maximized for different geometries. Similar to the divalent ChB complexes, the electrostatic contribution in the sp^2 chalcogens is maximized for the collinear geometry (X−E···A = 180°), where V_{min} at lp(A) points toward V_{max} at the σ-hole region of E (Figure S4). However, due to the presence of an empty π^*(EX) orbital (LUMO; Figure S4) lying lower in energy than the σ^*(EX) (LUMO+1), a stronger lp(A) to π^*(EX) CT can take place. This CT mechanism is maximized when lp(A) lays on top of the plane containing the Ch donor, close to a X−E···A right-angle. The geometry of F_2CE···NH_3 (**55**−**57**) and OCE···NH_3 (**58**−**60**) are determined by the electrostatic contribution. These complexes are characterized by a linear X−E···A geometry, weak ChBs ($n(EA)$ < 0.1), and small CT values (CT < 0.040). On the other hand, the geometries of FNE···NH_3 (**61**−**63**) are determined by covalent contributions, characterized by stronger ChBs ($n(EA)$ > 0.1) bent geometry X-E-A < 120° with larger CT values (CT > 0.080) and H_b < 0. The stronger covalent character of **61**−**63** is due to the higher electronegativity of N compared to C, which lowers the π^*(EX) orbital allowing a stronger lp(A) → σ^*(EX) CT to occur. Interesting to notice is that the σ-hole region in FNE is more strongly stretched in the π direction compared to F_2CE and OCE (Figure S2). Zhang, Ma, and Wang[85] found similar complexes, involving charge assisted XBs, where the geometries were not determined by the σ-hole position but by a the charge transfer from lp(A) → π^*(X−Cl). Here we show that this type of charge transfer mechanism can play a major role in the geometry of sp^2-hybridized ChB even for neutral complexes.

Charge Assisted ChB. The strongest ChBs found in the present study are realized for the charged complexes involving a cationic Ch donor ($n(EA)$ = 0.305 for **66** with ΔE = 37.6 kcal/mol) or an anionic Ch acceptor ($n(EA)$ = 0.348 for **80** with ΔE = 47.5 kcal/mol), with both, electrostatic and covalent contributions being magnified. For the cationic complexes, a more polarizable chalcogen (S < Se < Te) does not lead to a significative change in the ChB strength ($n(EA)$ = 0.287 (**64**), 0.300 (**65**), 0.305 (**66**) or ΔE = 36.9 (**64**), 37.5 (**65**), 37.6 (**66**)), whereas an electronegative ligand F collinear to the ChB still play an important role ($n(EA)$ = 0.287 (**64**) compared to $n(EA)$ = 0.166 (**67**)). Different from the neutral complexes, the ChB strength in **68** is not enhanced by the addition of a CN substituent ($n(EA)$ = 0.283 (**68**)).

Figure 9 gives the relative ChBs strength of a series of charged complexes formed with chloride. These ChBs are stronger than the ones found for NH_3, but still have similar strength trends with regard to the chalcogen (E = S < Se < Te), and the substituents (X = F_3C < F_2N < FO < F and Y = CF_2H *anti* < CF_2H *syn* < CN).

Notable is that not only FNE···Cl^- but also F_2CE···Cl^- complexes adopt a geometry of minimum energy with the C−E−Cl angle bent in the direction orthogonal to the plane

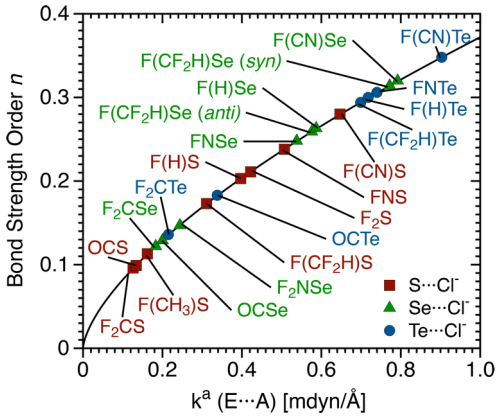

Figure 9. Power relationship between the relative bond strength order (BSO) n and the local stretching force constants k^a for complexes involving Cl^- and various Ch donors.

containing the Ch donor (C−E−Cl angle =125.3° (**81**), 142.4° (**82**), 158.1° (**83**)), maximizing the lp(Cl) → π^*(CE) charge transfer in detriment of the electrostatic interaction with the σ-hole collinear to the C-E bond (Figure S2).

ChB in Homodimers. In the symmetric homodimer complexes (**90**−**100**) both monomers are Ch donors and Ch acceptors. However, in **90**−**93** the chalcogen atoms involved donates and accepts electron density simultaneously, whereas complexes **94**−**100** form multiple ChBs. In the first case (**90**−**93**), two different types of bonding mechanisms are possible (i) the charge transfer can occur from the lp(E) orbital to the σ^*(EF) antibonding orbital (**90**, **91**) or (ii) the charge transfer can occur from the lp(E) to the π^*(EN) antibonding orbital (**92**, **93**). In both cases a skewed conformation is adopted to minimize lp(E)-lp(E) repulsion between the monomers. Figure 10 shows the orbitals involved in the CT mechanism (Figure

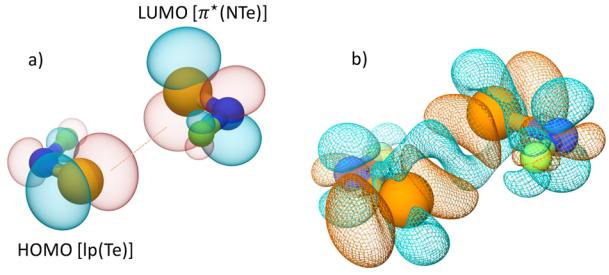

Figure 10. (a) Frontier molecular orbitals of $FNTe_2$ and (b) electron difference density distributions $\Delta\rho(r)$ of $FNTe_2$. $\Delta\rho(r)$ is plotted for an electron density surface of 0.001 au. Light blue regions indicate an increase in the electron density and brown regions a density decrease relative to the superimposed density of the monomers.

10a) and the electron difference density distribution (Figure 10b) for complex **93** ($FNTe_2$). The CT from lp(E) to π^*(NTe) and the lp(Te)−lp(Te) repulsion result in a density increase in the intermonomer region (light blue region between Te atoms in Figure 10) and a density depletion close to the Te atoms (large brown region close to Te atoms in Figure 10). To the best of our knowledge this is the first ChB homodimer found, where both monomers donate and accept charge via a lp(E) → π^*(EF) CT mechanism. This unusual new type of interaction may lead to novel supramolecular materials with unique geometric and electronic features. The possibility of

DOI: 10.1021/acs.jpca.7b06479
J. Phys. Chem. A 2017, 121, 6845−6862

similar interactions of this kind involving PnB is currently being investigated.

Figure 11 provides the ChB strength order for all symmetric homodimers **90**−**100**. Although the selenium complex of type

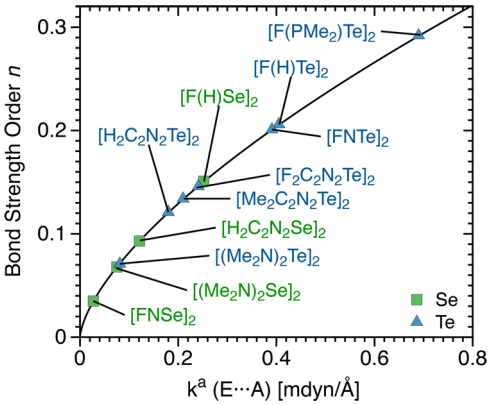

Figure 11. Power relationship between the relative bond strength order (BSO) n and the local stretching force constants k^a for the symmetric homodimers complexes.

ii (**92**) is much weaker than type i (**90**) ($n(EA)$ = 0.151(**90**) and 0.035(**92**), the tellurium complexes are of similar strength ($n(EA)$ = 0.206(**91**); 0.201(**93**)). Experimental studies reveal that complex **94** is a liquid, whereas **95** forms a highly reactive polymeric solid.[141] Both complexes have weak ChBs ($n(EA)$ = 0.068 (**94**); 0.071 (**95**); ΔE = 4.7 (**94**) 9.8 (**95**)). The ChBs in **95** can be strengthened by substituting the NMe_2 groups collinear to the ChB by F atoms and the nitrogen Ch acceptor atoms with phosphorus, leading to $(F(PMe_2)Te)_2$ (**96**). This complex has a strong ChB ($n(EA)$ = 0.292) and the highest binding energy among the neutral complexes (ΔE = 28.0 kcal/mol). However, **95** would form dimers, but not polymeric structures, due to the weak electron donor ability of the F atoms.

Better starting units forming relatively strong ChBs and polymeric structures are the selena- and telluradiazoles (**97**−**100**), where 1,2,5-telluradiazole dimers have stronger ChBs ($n(EA)$ = 0.121 (**98**) compared to 0.093 (**97**)). Although the difference between the BSO $n(EA)$ values of these complexes are relatively small, the increase in ΔE brought by the stronger ChBs in (**98**) is considerably large (ΔE = 13.6 (**98**) ; 6.3 (**97**) kcal/mol). Noteworthy is that both electron withdrawing (F) and electron donor (CH_3) substituents slightly enhance the strength of the ChB in telluradiazoles ($n(EA)$ = 0.146 (**99**) 0.134 (**100**) compared to 0.121(**98**)). The F substituents increase the electrostatic potential at the Te (V_{max} = 1.87 for $F_2C_2N_2Te$ compared to 1.30 eV for $H_2C_2N_2Te$) whereas the Me substituents strengthen the ChBs by increasing the polarizability of the monomers (α_{iso} = 101.3 for $Me_2C_2N_2Te$ compared to 73.6 Bohr^3 for $H_2C_2N_2Te$). A possible strategy to form strong polymeric structures based on ChBs is to increase the number of ChB contacts between monomers by fusing suitable ring structures to the telluradiazole monomers (increasing also its polarizability).

4. CONCLUSIONS AND OUTLOOK

In this work, we present for the first time a quantitative analysis of the intrinsic strength of 100 ChB based on the local stretching force constant and associated BSO, complemented by the analysis of binding energies, SAPT energy contributions, NBO charges, electrostatic potentials, isotropic polarizabilities, electron and energy density distributions, and difference density distributions. The following conclusions were obtained:

1 The ChB mechanism is composed of both, a covalent and an electrostatic part. The electrostatic part can be rationalized on the basis of the electrostatic potential of the Ch donors and the Ch acceptors, whereas the covalent part is associated with two different CT mechanisms. In divalent chalcogens, the CT is associated with lp(A) to σ^*(XE) delocalization, whereas in double bonded chalcogens it is associated with lp(A) to π^*(XE) delocalization. The latter CT mechanism can lead to the formation of strongly bent ChB complexes, which cannot be predicted by the inspection of the electrostatic potential of the monomers.

2 Based on BSO n values, we can identify three different classes of ChBs: weak ChBs ($n(EA) < 0.1$), normal ChBs ($0.1 < n(EA) < 0.2$), and strong ChBs $n(EA) > 0.2$. The strongest neutral ChB found (**96**) has an $n(EA)$ value of 0.292 (ΔE = 28.0 kcal/mol), whereas charge assisted ChBs reach values up to $n(EA)$ = 0.348 (ΔE = 47.5 kcal/mol) (**80**). The increase in the ChB strength is typically accompanied by a gradual increase in covalent character. Weak ChBs are dominated by electrostatic contributions and are characterized by $H_b \geq 0$, whereas all strong ChB are characterized by $H_b < 0$, which, according to the Cremer−Kraka criteria, indicates a dominant covalent character.

3 The ChB strength depends on the polarizability of the chalcogen atom (S < Se < Te), the electronegativity of the Ch donor substituent collinear to the ChB (CF_3 < NF_2 < OF < F), the electron withdrawing capability of the Ch donor substituent Y orthogonal to the ChB, and a small exchange−repulsion between lp(A) and the Y substituent (e.g., if Y = CF_3 is rotated to a *syn* conformation, where the F atom in the mirror plane of the complex is moved away from lp(A) there is an increase in the ChB strength).

4 The Ch acceptor also exerts a strong influence on the strength of the ChB. For a given period of the PT, the decrease in the electronegativity of the Ch acceptor atom A leads to an increase in the ChB strength due to the higher donor ability of lp(A) and decreased electrostatic potential. Descending within a group of the PT the ChB becomes weaker due to the increased diffuseness of lp(A). Strong ChB involving heteroatoms of lower periods can be envisioned by adding substituents that effectively contract lp(A) (e.g., PMe_3).

5 3c−4e character of chalcogen bonds can play an important role in strong ChB complexes, reaching up to 56% for the neutral complex **28** and 69% for the charged assisted complex **76** *syn*. However, these values are considerably lower than the ones found for halogen bonds.[75,97,98] CT and 3c−4e character in ChBs are reduced (in comparison with XB) due to the lower electronegativity of chalcogens compared to the halogens (resulting in σ^*(XE) orbitals of higher energy thus a larger $\Delta\epsilon$(2e) energy gap) and due to the bent conformation adopted by chalcogen complexes (resulting in a less effective overlap between lp(A) and σ^*(XE) orbitals.

DOI: 10.1021/acs.jpca.7b06479
J. Phys. Chem. A 2017, 121, 6845−6862

6 Multiple ChBs in homodimers (**94**−**100**) can result in an extra stabilization. For example complex **96** has a ΔE = 28.0 kcal/mol, comparable to the strongest neutral XB complexes previously studied[75,97,98] and stronger than that of neutral hydrogen bonds[142] and pnicogen bonds in general.[129]

7 We describe for the first time a symmetric homodimer, where both monomers donate charge from lp(A) to π^*(XE) simultaneously. This new type of interaction may lead to the development of polymers with unique architecture and electronic properties.

8 New polymeric structures based on ChB should focus on molecules that can make multiple ChB contacts such as 1,2,5-Telluradiazole. The stability of these complexes can be improved by fusing rings to increase the polarizability and the number of possible ChB between the monomers.

By rationalizing the intrinsic strength of an extensive set of 100 ChBs on the basis of the analysis of the essential electronic effects and their interplay with the covalent and electrostatic contributions, we provide a concise description of the ChB, which is of general applicability and may serve as the basis for the design of larger and more complex ChB structures.

■ ASSOCIATED CONTENT

Supporting Information

This material is avaliable free of charge via the Internet at The Supporting Information is available free of charge on the ACS Publications website at DOI: 10.1021/acs.jpca.7b06479.

Binding energies (ΔE), ChB distances r(EA), and ChB force constants k^a(EA) for 12 complexes calculated using CCSD(T), MP2, and 3 DFTs (Tables S1−S3), SAPT0 energy component for complexes **43**, **46**, and **48** (Table S4), frontier molecular orbitals, orbital energies, and molecules electrostatic potential for all Ch donors and Ch acceptors (Figures S1−S4), a comparison of the ChB BSO values and ΔE (Figure S5), interaction energies (Figure S6), density ρ_b(EA) (Figure S7) and ΔE(del) (Figure S8), schematic representation of complexes and monomers with geometric parameters (Figures S9−S13), and NPA partial atomic charges (Figures S14−S17). (PDF)

■ AUTHOR INFORMATION

Corresponding Author

*(E.K.) E-mail: ekraka@smu.edu.

ORCID

Dieter Cremer: 0000-0002-6213-5555

Elfi Kraka: 0000-0002-9658-5626

Notes

The authors declare no competing financial interest.

†In memoriam.

■ ACKNOWLEDGMENTS

This work was financially supported by the National Science Foundation, Grant CHE 1464906. We thank SMU for providing computational resources. The authors acknowledge financial support by CAPES (Brazil Fellowship Grant BEX 9534-13-0).

■ REFERENCES

(1) Alcock, N. W.; Emeleus, H. J.; Sharpe, A. G. Secondary Bonding to Nonmetallic Elements. *Adv. Inorg. Chem. Radiochem.* **1972**, *15*, 1−58.

(2) Cozzolino, A. F.; Elder, P. J.; Vargas-Baca, I. A survey of tellurium-centered secondary-bonding supramolecular synthons. *Coord. Chem. Rev.* **2011**, *255*, 1426−1438.

(3) Landrum, G. A.; Hoffmann, R. Secondary bonding between chalcogens or pnicogens and halogens. *Angew. Chem., Int. Ed.* **1998**, *37*, 1887−1890.

(4) Werz, D. B.; Gleiter, R.; Rominger, F. Nanotube formation favored by chalcogen-chalcogen interactions. *J. Am. Chem. Soc.* **2002**, *124*, 10638−10639.

(5) Gleiter, R.; Werz, D. B.; Rausch, B. J. A world beyond hydrogen bonds? Chalcogen-chalcogen interactions yielding tubular structures. *Chem. - Eur. J.* **2003**, *9*, 2676−2683.

(6) Gleiter, R.; Werz, D. B. Elastic cycles as flexible hosts: How tubes built by cyclic chalcogenaalkynes individually host their guests. *Chem. Lett.* **2005**, *34*, 126−131.

(7) Ho, P. C.; Szydlowski, P.; Sinclair, J.; Elder, P. J. W.; Kübel, J.; Gendy, C.; Lee, L. M.; Jenkins, H.; Britten, J. F.; Morim, D. R.; et al. Supramolecular macrocycles reversibly assembled by Te(···)O chalcogen bonding. *Nat. Commun.* **2016**, *7*, 11299.

(8) Lim, J. Y. C.; Marques, I.; Thompson, A. L.; Christensen, K. E.; Felix, V.; Beer, P. D. Chalcogen bonding macrocycles and [2]rotaxanes for anion recognition. *J. Am. Chem. Soc.* **2017**, *139*, 3122−3133.

(9) Allan, R. E.; Gornitzka, H.; Karcher, J.; Paver, M. A.; Rennie, M.-A.; Russell, C. A.; Raithby, P. R.; Stalke, D.; Steiner, A.; Wright, D. S. Structure and reactivity of $Te(NMe_2)_2\infty$; application to the preparation of metalloorganic tellurium(II) compounds. *J. Chem. Soc., Dalton Trans.* **1996**, 1727−1730.

(10) Eichstaedt, K.; Wasilewska, A.; Wicher, B.; Gdaniec, M.; Połoński, T. Supramolecular synthesis based on a combination of Se···N secondary bonding interactions with hydrogen and halogen bonds. *Cryst. Growth Des.* **2016**, *16*, 1282−1293.

(11) Pavan, M. S.; Jana, A. K.; Natarajan, S.; Guru Row, T. N. Halogen bonding and chalcogen bonding in 4,7-dibromo-5,6-dinitro-2,1,3-benzothiadiazole. *J. Phys. Chem. B* **2015**, *119*, 11382−11390.

(12) Kremer, A.; Fermi, A.; Biot, N.; Wouters, J.; Bonifazi, D. Supramolecular wiring of benzo-1,3-chalcogenazoles through programmed chalcogen bonding interactions. *Chem. - Eur. J.* **2016**, *22*, 5665−5675.

(13) Tsuzuki, S.; Sato, N. Origin of attraction in chalgogen-nitrogen interaction of 1,2,5-chalcogenadiazole dimers. *J. Phys. Chem. B* **2013**, *117*, 6849−6855.

(14) Pati, P. B.; Zade, S. S. Benzoselenadiazole containing donor-acceptor-donor small molecules: Nonbonding interactions, packing patterns, and optoelectronic properties. *Cryst. Growth Des.* **2014**, *14*, 1695−1700.

(15) Lonchakov, A. V.; Rakitin, O. A.; Gritsan, N. P.; Zibarev, A. V. Breathing some new life into an old topic: Chalcogen-nitrogen π-heterocycles as electron acceptors. *Molecules* **2013**, *18*, 9850−9900.

(16) Semenov, N. A.; Lonchakov, A. V.; Pushkarevsky, N. A.; Suturina, E. A.; Korolev, V. V.; Lork, E.; Vasiliev, V. G.; Konchenko, S. N.; Beckmann, J.; Gritsan, N. P.; et al. Coordination of halide and chalcogenolate anions to heavier 1,2,5-chalcogenadiazoles: Experiment and theory. *Organometallics* **2014**, *33*, 4302−4314.

(17) Cozzolino, A. F.; Yang, Q.; Vargas-Baca, I. Engineering second-order nonlinear optical activity by means of a noncentrosymmetric distortion of the [Te-N]2 supramolecular synthon. *Cryst. Growth Des.* **2010**, *10*, 4959−4964.

(18) Lindner, B. D.; Coombs, B. A.; Schaffroth, M.; Engelhart, J. U.; Tverskoy, O.; Rominger, F.; Hamburger, M.; Bunz, U. H. F. From thia- to selenadiazoles: Changing interaction priority. *Org. Lett.* **2013**, *15*, 666−669.

(19) Iwaoka, M.; Takemoto, S.; Okada, M.; Tomoda, S. Weak nonbonded S···X (X = O, N, and S) interactions in proteins. Statistical and theoretical studies. *Bull. Chem. Soc. Jpn.* **2002**, *75*, 1611−1625.

DOI: 10.1021/acs.jpca.7b06479
J. Phys. Chem. A 2017, 121, 6845−6862

(20) Iwaoka, M.; Takemoto, S.; Tomoda, S. Statistical and theoretical investigations on the directionality of nonbonded S···O interactions. Implications for molecular design and protein engineering. *J. Am. Chem. Soc.* **2002**, *124*, 10613−10620.
(21) Manna, D.; Mugesh, G. Regioselective deiodination of thyroxine by iodothyronine deiodinase mimics: An unusual mechanistic pathway involving cooperative chalcogen and halogen bonding. *J. Am. Chem. Soc.* **2012**, *134*, 4269−4279.
(22) Benz, S.; López-Andarias, J.; Mareda, J.; Sakai, N.; Matile, S. Catalysis with chalcogen bonds. *Angew. Chem., Int. Ed.* **2017**, *56*, 812−815.
(23) Mugesh, G.; Panda, A.; Kumar, S.; Apte, S. D.; Singh, H. B.; Butcher, R. J. Intramolecularly coordinated diorganyl ditellurides:? Thiol peroxidase-like antioxidants. *Organometallics* **2002**, *21*, 884−892.
(24) Nziko, V. d. P. N.; Scheiner, S. S···π chalcogen bonds between SF_2 or SF_4 and C-C multiple bonds. *J. Phys. Chem. A* **2015**, *119*, 5889−5897.
(25) Benz, S.; Macchione, M.; Verolet, Q.; Mareda, J.; Sakai, N.; Matile, S. Anion transport with chalcogen bonds. *J. Am. Chem. Soc.* **2016**, *138*, 9093−9096.
(26) Garrett, G. E.; Carrera, E. I.; Seferos, D. S.; Taylor, M. S. Anion recognition by a bidentate chalcogen bond donor. *Chem. Commun.* **2016**, *52*, 9881−9884.
(27) Scheiner, S. Highly selective halide receptors based on chalcogen, pnicogen, and tetrel Bonds. *Chem. - Eur. J.* **2016**, *22*, 18850−18858.
(28) Fick, R. J.; Kroner, G. M.; Nepal, B.; Magnani, R.; Horowitz, S.; Houtz, R. L.; Scheiner, S.; Trievel, R. C. Sulfur-oxygen chalcogen bonding mediates AdoMet recognition in the lysine methyltransferase SET7/9. *ACS Chem. Biol.* **2016**, *11*, 748−754.
(29) Thomas, S. P.; Jayatilaka, D.; Guru Row, T. N. S···O chalcogen bonding in sulfa drugs: Insights from multipole charge density and X-ray wavefunction of acetazolamide. *Phys. Chem. Chem. Phys.* **2015**, *17*, 25411−25420.
(30) Thomas, S. P.; Satheeshkumar, K.; Mugesh, G.; Guru Row, T. N. Unusually short chalcogen bonds involving organoselenium: Insights into the Se-N Bond cleavage mechanism of the antioxidant ebselen and analogues. *Chem. - Eur. J.* **2015**, *21*, 6793−6800.
(31) Beno, B. R.; Yeung, K.-S.; Bartberger, M. D.; Pennington, L. D.; Meanwell, N. A. A Survey of the role of noncovalent sulfur interactions in drug design. *J. Med. Chem.* **2015**, *58*, 4383−4438.
(32) Nagao, Y.; Hirata, T.; Goto, S.; Sano, S.; Kakehi, A.; Iizuka, K.; Shiro, M. Intramolecular nonbonded S···O interaction recognized in (acylimino)thiadiazoline derivatives as angiotensin II receptor antagonists and related compounds. *J. Am. Chem. Soc.* **1998**, *120*, 3104−3110.
(33) Iwaoka, M.; Tomoda, S. Nature of the intramolecular Se···N nonbonded interaction of 2-selenobenzylamine derivatives. An experimental evaluation by ^1H, ^77Se, and ^15N NMR spectroscopy. *J. Am. Chem. Soc.* **1996**, *118*, 8077−8084.
(34) Iwaoka, M.; Komatsu, H.; Katsuda, T.; Tomoda, S. Quantitative evaluation of weak nonbonded Se···F interactions and their remarkable nature as orbital interactions. *J. Am. Chem. Soc.* **2002**, *124*, 1902−1909.
(35) Iwaoka, M.; Komatsu, H.; Katsuda, T.; Tomoda, S. Nature of nonbonded Se···O interactions characterized by ^17O NMR spectroscopy and NBO and AIM analyses. *J. Am. Chem. Soc.* **2004**, *126*, 5309−5317.
(36) Iwaoka, M.; Katsuda, T.; Komatsu, H.; Tomoda, S. Experimental and theoretical studies on the nature of weak nonbonded interactions between divalent selenium and halogen atoms. *J. Org. Chem.* **2005**, *70*, 321−327.
(37) Rosenfield, R. E.; Parthasarathy, R.; Dunitz, J. D. Directional preferences of nonbonded atomic contacts with divalent sulfur. 1. Electrophiles and nucleophiles. *J. Am. Chem. Soc.* **1977**, *99*, 4860−4862.
(38) Bleiholder, C.; Werz, D. B.; Köppel, H.; Gleiter, R. Theoretical investigations on chalcogen-chalcogen interactions: What makes these nonbonded interactions bonding? *J. Am. Chem. Soc.* **2006**, *128*, 2666−2674.
(39) Bleiholder, C.; Gleiter, R.; Werz, D. B.; Köppel, H. Theoretical investigations on heteronuclear chalcogen-chalcogen interactions: On the nature of weak bonds between chalcogen centers. *Inorg. Chem.* **2007**, *46*, 2249−2260.
(40) Azofra, L. M.; Alkorta, I.; Scheiner, S. Chalcogen bonds in complexes of SOXY (X, Y = F, Cl) with nitrogen bases. *J. Phys. Chem. A* **2015**, *119*, 535−541.
(41) Scheiner, S. Comparison of CH···O, SH···O, chalcogen, and tetrel bonds formed by neutral and cationic sulfur-containing compounds. *J. Phys. Chem. A* **2015**, *119*, 9189−9199.
(42) Nziko, V. d. P. N.; Scheiner, S. Chalcogen bonding between tetravalent SF_4 and amines. *J. Phys. Chem. A* **2014**, *118*, 10849−10856.
(43) Esrafili, M. D.; Mohammadian-Sabet, F. σ-Hole bond tunability in YO_2X_2:NH_3 and YO_2X_2:H_2O complexes (X = F, Cl, Br; Y = S, Se): Trends and theoretical aspects. *Struct. Chem.* **2016**, *27*, 617−625.
(44) Esrafili, M. D.; Mohammadian-Sabet, F. An ab initio study on chalcogen-chalcogen bond interactions in cyclic $(SHX)_3$ complexes (X = F, Cl, CN, NC, CCH, OH, OCH_3, NH_2). *Chem. Phys. Lett.* **2015**, *628*, 71−75.
(45) Esrafili, M. D.; Mohammadian-Sabet, F. Homonuclear chalcogen-chalcogen bond interactions in complexes pairing YO_3 and YHX molecules (Y = S, Se; X = H, Cl, Br, CCH, NC, OH, OCH_3): Influence of substitution and cooperativity. *Int. J. Quantum Chem.* **2016**, *116*, 529−536.
(46) Esrafili, M. D.; Nurazar, R. Chalcogen bonds formed through π-holes: SO_3 complexes with nitrogen and phosphorus bases. *Mol. Phys.* **2016**, *114*, 276−282.
(47) Esrafili, M. D.; Mohammadian-Sabet, F. An ab initio study on cationic chalcogen bond interactions between $F_{3-n}H_nS^+$ (n = 0−2) and nitrogen bases. *Chem. Phys. Lett.* **2016**, *645*, 32−37.
(48) Zierkiewicz, W.; Fanfrlík, J.; Hobza, P.; Michalska, D.; Zeegers-Huyskens, T. Ab initio and DFT studies of the interaction between carbonyl and thiocarbonyl groups. The role of S···O chalcogen bonds. *Theor. Chem. Acc.* **2016**, *135*, 217.
(49) Zhao, Q.; Feng, D.; Sun, Y.; Hao, J.; Cai, Z. Theoretical investigations on the weak chalcogen-bonded complexes with nonbonded C = S···CH_2 interactions: Singlet carbene as an electron donor. *Int. J. Quantum Chem.* **2011**, *111*, 3881−3887.
(50) Shukla, R.; Chopra, D. Crystallographic and theoretical investigation on the nature and characteristics of type I C-S···S-C interactions. *Cryst. Growth Des.* **2016**, *16*, 6734−6742.
(51) Khan, I.; Panini, P.; Khan, S. U.-D.; Rana, U. A.; Andleeb, H.; Chopra, D.; Hameed, S.; Simpson, J. Exploiting the role of molecular electrostatic potential, deformation density, topology, and energetics in the characterization of S···N and Cl···N supramolecular motifs in crystalline triazolothiadiazoles. *Cryst. Growth Des.* **2016**, *16*, 1371−1386.
(52) Nziko, V. d. P. N.; Scheiner, S. Intramolecular S···O chalcogen bond as stabilizing factor in geometry of substituted phenyl-SF_3 molecules. *J. Org. Chem.* **2015**, *80*, 2356−2363.
(53) Wang, C.; Guan, L.; Danovich, D.; Shaik, S.; Mo, Y. The origins of the directionality of noncovalent intermolecular interactions. *J. Comput. Chem.* **2016**, *37*, 34−45.
(54) Zhang, X.; Gong, Z.; Li, J.; Lu, T. Intermolecular sulfur···oxygen interactions: Theoretical and statistical investigations. *J. Chem. Inf. Model.* **2015**, *55*, 2138−2153.
(55) Si, M. K.; Ganguly, B. Computational evidence that hyperconjugative orbital interactions are responsible for the stability of intramolecular Te···O/Te···S non-covalent interactions and comparable to hydrogen bonds in quasi-cyclic systems. *New J. Chem.* **2016**, *40*, 9132−9138.
(56) Esrafili, M. D.; Mohammadian-Sabet, F. Bifurcated chalcogen bonds: A theoretical study on the structure, strength and bonding properties. *Chem. Phys. Lett.* **2015**, *634*, 210−215.
(57) Adhikari, U.; Scheiner, S. Effects of charge and substituent on the S···N chalcogen bond. *J. Phys. Chem. A* **2014**, *118*, 3183−3192.
(58) Esrafili, M. D.; Mohammadian-Sabet, F. Does single-electron chalcogen bond exist? Some theoretical insights. *J. Mol. Model.* **2015**, *21*, 65.

DOI: 10.1021/acs.jpca.7b06479
J. Phys. Chem. A 2017, 121, 6845−6862

(59) Esrafili, M. D.; Mohammadian-Sabet, F. Prediction and characterisation of a chalcogen···π interaction with acetylene as a potential electron donor in XHS···HCCH and XHSe···HCCH (X = F, Cl, Br, CN, OH, OCH_3, NH_2, CH_3) σ-hole complexes. *Mol. Phys.* **2015**, *113*, 3559−3566.
(60) Shukla, R.; Chopra, D. Pnicogen bonds or chalcogen bonds: Exploiting the effect of substitution on the formation of P···Se noncovalent bonds. *Phys. Chem. Chem. Phys.* **2016**, *18*, 13820−13829.
(61) Haberhauer, G.; Gleiter, R. Double pancake versus long chalcogen-chalcogen bonds in six-membered C,N,S-heterocycles. *Chem. - Eur. J.* **2016**, *22*, 8646−8653.
(62) Fanfrlik, J.; Prada, A.; Padelkova, Z.; Pecina, A.; Machacek, J.; Lepsik, M.; Holub, J.; Ruzicka, A.; Hnyk, D.; Hobza, P. The dominant role of chalcogen bonding in the crystal packing of 2D/3D aromatics. *Angew. Chem., Int. Ed.* **2014**, *53*, 10139−10142.
(63) Antonijevic, I. S.; Janjic, G. V.; Milcic, M. K.; Zaric, S. D. Preferred geometries and energies of sulfur-sulfur interactions in crystal structures. *Cryst. Growth Des.* **2016**, *16*, 632−639.
(64) Politzer, P.; Murray, J. S.; Clark, T. Halogen bonding: An electrostatically-driven highly directional noncovalent interaction. *Phys. Chem. Chem. Phys.* **2010**, *12*, 7748−7757.
(65) Kolar, M.; Hostas, J.; Hobza, P. The strength and directionality of a halogen bond are co-determined by the magnitude and size of the σ-hole. *Phys. Chem. Chem. Phys.* **2014**, *16*, 9987−9996.
(66) Grant Hill, J.; Legon, A. C. On the directionality and non-linearity of halogen and hydrogen bonds. *Phys. Chem. Chem. Phys.* **2015**, *17*, 858−867.
(67) Stone, A. J. Are halogen bonded structures electrostatically driven? *J. Am. Chem. Soc.* **2013**, *135*, 7005−7009.
(68) Pecina, A.; Lepsik, M.; Hnyk, D.; Hobza, P.; Fanfrlik, J. Chalcogen and pnicogen bonds in complexes of neutral icosahedral and bicapped square-antiprismatic heteroboranes. *J. Phys. Chem. A* **2015**, *119*, 1388−1395.
(69) Joy, J.; Jose, A.; Jemmis, E. D. Continuum in the X-Z-Y weak bonds: Z= main group elements. *J. Comput. Chem.* **2016**, *37*, 270−279.
(70) Nepal, B.; Scheiner, S. Long-range behavior of noncovalent bonds. Neutral and charged H-bonds, pnicogen, chalcogen, and halogen bonds. *Chem. Phys.* **2015**, *456*, 34−40.
(71) Adhikari, U.; Scheiner, S. Substituent effects on Cl···N, S···N, and P···N noncovalent bonds. *J. Phys. Chem. A* **2012**, *116*, 3487−3497.
(72) Scheiner, S. Detailed comparison of the pnicogen bond with chalcogen, halogen, and hydrogen bonds. *Int. J. Quantum Chem.* **2013**, *113*, 1609−1620.
(73) Asiabar, B. M.; Esrafili, M. D.; Mohammadian-Sabet, F.; Sobhi, H. R.; Javaheri, M. An ab initio study on the concerted interaction between chalcogen and pnicogen bonds. *J. Mol. Model.* **2014**, *20*, 2545.
(74) Esrafili, M. D.; Akhgarpour, H. An ab initio study on competition between pnicogen and chalcogen bond interactions in binary XHS:PH_2X complexes (X = F, Cl, CCH, COH, CH_3, OH, OCH_3 and NH_2). *Mol. Phys.* **2016**, *114*, 1847−1855.
(75) Oliveira, V.; Kraka, E.; Cremer, D. The intrinsic strength of the halogen bond: Electrostatic and covalent contributions described by coupled cluster theory. *Phys. Chem. Chem. Phys.* **2016**, *18*, 33031−33046.
(76) Fang, Y.; Li, A. Y.; Ma, F. Y. A comparative study of the chalcogen bond, halogen bond and hydrogen bond S···O/Cl/H formed between SHX and HOCl. *J. Mol. Model.* **2015**, *21*, 61.
(77) Guo, X.; Liu, Y.-W.; Li, Q.-Z.; Li, W.-Z.; Cheng, J.-B. Competition and cooperativity between tetrel bond and chalcogen bond in complexes involving F_2CX (X = Se and Te). *Chem. Phys. Lett.* **2015**, *620*, 7−12.
(78) Guo, X.; An, X.; Li, Q. Se···N chalcogen bond and Se···X halogen bond involving F_2CSe: Influence of hybridization, substitution, and cooperativity. *J. Phys. Chem. A* **2015**, *119*, 3518−3527.
(79) Li, Q.-Z. Z.; Li, R.; Guo, P.; Li, H.; Li, W.-Z. Z.; Cheng, J.-B. B. Competition of chalcogen bond, halogen bond, and hydrogen bond in SCS-HOX and SeC-SeHOX (X = Cl and Br) complexes. *Comput. Theor. Chem.* **2012**, *980*, 56−61.
(80) Bauza, A.; Quinonero, D.; Deya, P. M.; Frontera, A. Halogen bonding versus chalcogen and pnicogen bonding: A combined Cambridge structural database and theoretical study. *CrystEngComm* **2013**, *15*, 3137−3144.
(81) Sanz, P.; Yáñez, M.; Mó, O. Competition between X···H···Y intramolecular hydrogen bonds and X···Y (X = O, S, and Y = Se, Te) chalcogen-chalcogen interactions. *J. Phys. Chem. A* **2002**, *106*, 4661−4668.
(82) Sanz, P.; Yáñez, M.; Mó, O. The role of chalcogen-chalcogen interactions in the intrinsic basicity and acidity of β-chalcogenovinyl-(thio)aldehydes HC(=X)-CH = CH-CYH (X = O, S; Y = Se, Te). *Chem. - Eur. J.* **2002**, *8*, 3999−4007.
(83) Clark, T.; Hennemann, M.; Murray, J.; Politzer, P. Halogen bonding: The σ-hole. *J. Mol. Model.* **2007**, *13*, 291−296.
(84) Politzer, P.; Murray, J.; Concha, M. Halogen bonding and the design of new materials: Organic bromides, chlorides and perhaps even fluorides as donors. *J. Mol. Model.* **2007**, *13*, 643−650.
(85) Zhang, Y.; Ma, N.; Wang, W. A new class of halogen bonds that avoids the σ-hole. *Chem. Phys. Lett.* **2012**, *532*, 27−30.
(86) Ramasami, P.; Ford, T. A. Chalcogen-bonded complexes. Selenium-bound adducts of NH_3, H_2O, PH_3, and H_2S with OCSe, SCSe, and CSe_2. *J. Mol. Model.* **2015**, *21*, 35.
(87) Esrafili, M. D.; Mohammadian-Sabet, F. Ab initio calculations of cooperativity effects on chalcogen bonding: Linear clusters of $(OCS)_{2-8}$ and $(OCSe)_{2-8}$. *Struct. Chem.* **2015**, *26*, 199−206.
(88) Wang, W.; Ji, B.; Zhang, Y. Chalcogen bond: A sister noncovalent bond to halogen bond. *J. Phys. Chem. A* **2009**, *113*, 8132−8135.
(89) Alikhani, E.; Fuster, F.; Madebene, B.; Grabowski, S. J. Topological reaction sites - Very strong chalcogen bonds. *Phys. Chem. Chem. Phys.* **2014**, *16*, 2430−2442.
(90) Cozzolino, A. F.; Vargas-Baca, I.; Mansour, S.; Mahmoudkhani, A. H. The nature of the supramolecular association of 1,2,5-chalcogenadiazoles. *J. Am. Chem. Soc.* **2005**, *127*, 3184−3190.
(91) Esrafili, M. D.; Vakili, M. Halogen bonds enhanced by σ-hole and π-hole interactions: A comparative study on cooperativity and competition effects between X···N and S···N interactions in H_3N···XCN···SF_2 and H_3N···XCN···SO_2 complexes (X = F, Cl, Br and I. *J. Mol. Model.* **2014**, *20*, 2291.
(92) Esseffar, M.; Herrero, R.; Quintanilla, E.; Dávalos, J. Z.; Jiménez, P.; Abboud, J.-L. M.; Yáñez, M.; Mó, O. Activation of the disulfide bond and chalcogen-chalcogen interactions: An experimental (FTICR) and computational study. *Chem. - Eur. J.* **2007**, *13*, 1796−1803.
(93) Cozzolino, A. F.; Vargas-Baca, I. The supramolecular chemistry of 1,2,5-chalcogenadiazoles. *J. Organomet. Chem.* **2007**, *692*, 2654−2657.
(94) Cozzolino, A. F.; Elder, P. J. W.; Lee, L. M.; Vargas-Baca, I. The role of the Lewis acid-base properties in the supramolecular association of 1,2,5-chalcogenadiazoles. *Can. J. Chem.* **2013**, *91*, 338−347.
(95) Cozzolino, A. F.; Britten, J. F.; Vargas-Baca, I. The effect of steric hindrance on the association of telluradiazoles through Te-N secondary bonding interactions. *Cryst. Growth Des.* **2006**, *6*, 181−186.
(96) Cozzolino, A. F.; Whitfield, P. S.; Vargas-Baca, I. Supramolecular chromotropism of the crystalline phases of 4,5,6,7-tetrafluorobenzo-2,1,3-telluradiazole. *J. Am. Chem. Soc.* **2010**, *132*, 17265−17270.
(97) Oliveira, V.; Kraka, E.; Cremer, D. Quantitative assessment of halogen bonding utilizing vibrational spectroscopy. *Inorg. Chem.* **2017**, *56*, 488−502.
(98) Li, Y.; Oliveira, V.; Tang, C.; Cremer, D.; Liu, C.; Ma, J. The peculiar role of the Au_3 unit in Au_m clusters: σ-aromaticity of the Au_5Zn^+ Ion. *Inorg. Chem.* **2017**, *56*, 5793−5803.
(99) Kraka, E.; Setiawan, D.; Cremer, D. Re-evaluation of the bond length - bond strength rule: The stronger bond is not always the shorter bond. *J. Comput. Chem.* **2016**, *37*, 130−142.
(100) Setiawan, D.; Kraka, E.; Cremer, D. Hidden bond anomalies: The peculiar case of the fluorinated amine chalcogenides. *J. Phys. Chem. A* **2015**, *119*, 9541−9556.

DOI: 10.1021/acs.jpca.7b06479
J. Phys. Chem. A 2017, 121, 6845−6862

(101) Kraka, E.; Larsson, J. A.; Cremer, D. In *Computational spectroscopy: Methods, experiments and applications*; Grunenberg, J., Ed.; Wiley: New York, 2010; pp 105−149.
(102) Konkoli, Z.; Cremer, D. A new way of analyzing vibrational spectra I. Derivation of adiabatic internal modes. *Int. J. Quantum Chem.* **1998**, *67*, 1−9.
(103) Cremer, D.; Larsson, J. A.; Kraka, E.; et al. New developments in the analysis of vibrational spectra On the use of adiabatic internal vibrational modes. *Theor. Comput. Chem.* **1998**, *5*, 259−327.
(104) Zou, W.; Kalescky, R.; Kraka, E.; Cremer, D. Relating normal vibrational modes to local vibrational modes with the help of an adiabatic connection scheme. *J. Chem. Phys.* **2012**, *137*, 084114.
(105) Wilson, E. B.; Decius, J. C.; Cross, P. C. *Molecular vibrations. The theory of infrared and Raman vibrational spectra*; McGraw-Hill: New York, 1955.
(106) Cremer, D.; Kraka, E. Generalization of the Tolman electronic parameter: The metal-ligand electronic parameter and the intrinsic strength of the metal-ligand bond. *Dalton Trans.* **2017**, *46*, 8323.
(107) Møller, C.; Plesset, M. S. Note on an approximation treatment for many-electron systems. *Phys. Rev.* **1934**, *46*, 618−622.
(108) Becke, A. D. Density-functional thermochemistry. III. The role of exact exchange. *J. Chem. Phys.* **1993**, *98*, 5648−5652.
(109) Stephens, P. J.; Devlin, F. J.; Chabalowski, C. F.; Frisch, M. J. Ab initio calculation of vibrational absorption and circular dichroism spectra using density functional force fields. *J. Phys. Chem.* **1994**, *98*, 11623−11627.
(110) Grimme, S.; Antony, J.; Ehrlich, S.; Krieg, H. A consistent and accurate ab initio parametrization of density functional dispersion correction (DFT-D) for the 94 elements H-Pu. *J. Chem. Phys.* **2010**, *132*, 154104.
(111) Grimme, S.; Ehrlich, S.; Goerigk, L. Effect of the damping function in dispersion corrected density functional theory. *J. Comput. Chem.* **2011**, *32*, 1456−1465.
(112) Zhao, Y.; Truhlar, D. G. The M06 suite of density functionals for main group thermochemistry, thermochemical kinetics, noncovalent interactions, excited states, and transition elements: Two new functionals and systematic testing of four M06-class functionals and 12 other functionals. *Theor. Chem. Acc.* **2008**, *120*, 215−241.
(113) Chai, J. D.; Head-Gordon, M. Long-range corrected hybrid density functionals with damped atom-atom dispersion corrections. *Phys. Chem. Chem. Phys.* **2008**, *10*, 6615.
(114) Chai, J. D.; Head-Gordon, M. Systematic optimization of long-range corrected hybrid density functionals. *J. Chem. Phys.* **2008**, *128*, 084106.
(115) Raghavachari, K.; Trucks, G. W.; Pople, J. A.; Head-Gordon, M. A fifth-order perturbation comparison of electron correlation theories. *Chem. Phys. Lett.* **1989**, *157*, 479−483.
(116) Woon, D.; Dunning, T. J. Gaussian basis sets for use in correlated molecular calculations. IV. Calculation of static electrical response properties. *J. Chem. Phys.* **1994**, *100*, 2975−2988.
(117) Dunning, T. Gaussian basis sets for use in correlated molecular calculations. I. The atoms boron through neon and hydrogen. *J. Chem. Phys.* **1989**, *90*, 1007−1023.
(118) Woon, D.; Dunning, T. Gaussian basis sets for use in correlated molecular calculations. III. The atoms aluminum through argon. *J. Chem. Phys.* **1993**, *98*, 1358−1371.
(119) Boys, S.; Bernardi, F. The calculation of small molecular interactions by the differences of separate total energies. *Mol. Phys.* **1970**, *19*, 553−566.
(120) Grafenstein, J.; Cremer, D. Efficient DFT integrations by locally augmented radial grids. *J. Chem. Phys.* **2007**, *127*, 164113.
(121) Peterson, K. A.; Figgen, D.; Goll, E.; Stoll, H.; Dolg, M. Systematically convergent basis sets with relativistic pseudopotentials. II. Small-core pseudopotentials and correlation consistent basis sets for the post-d group 16−18 elements. *J. Chem. Phys.* **2003**, *119*, 11113−11123.
(122) Kalescky, R.; Kraka, E.; Cremer, D. Identification of the strongest bonds in chemistry. *J. Phys. Chem. A* **2013**, *117*, 8981−8995.
(123) Chivers, T.; Laitinen, R. S. Tellurium: A maverick among the chalcogens. *Chem. Soc. Rev.* **2015**, *44*, 1725−1739.
(124) Nakanishi, W.; Hayashi, S.; Pitak, M. B.; Hursthouse, M. B.; Coles, S. J. Dynamic and static behaviors of N-Z-N σ(3c−4e) (Z = S, Se, and Te) interactions: Atoms-in-molecules dual functional analysis with high-resolution X-ray diffraction determination of electron densities for 2-(2-pyridylimino)-2H-1,2,4-thiadiazolo[2,3-a]pyrid. *J. Phys. Chem. A* **2011**, *115*, 11775−11787.
(125) Gleiter, R.; Haberhauer, G. Long chalcogen-chalcogen bonds in electron-rich two and four center bonds: Combination of π- and σ-aromaticity to a three-dimensional σ/π-aromaticity. *J. Org. Chem.* **2014**, *79*, 7543−7552.
(126) Cremer, D.; Kraka, E. A description of the chemical bond in terms of local properties of electron density and energy. *Croat. Chem. Acta* **1984**, *57*, 1259−1281.
(127) Cremer, D.; Kraka, E. Chemical bonds without bonding electron density - Does the difference electron density analysis suffice for a description of the chemical bond? *Angew. Chem., Int. Ed. Engl.* **1984**, *23*, 627−628.
(128) Kraka, E.; Cremer, D.; Maksic, Z. Chemical Implication of Local Features of the Electron Density Distribution. *Theoretical models of chemical bonding. The concept of the chemical bond* **1990**, *2*, 453−542.
(129) Setiawan, D.; Kraka, E.; Cremer, D. Strength of the pnicogen bond in complexes involving group Va elements N, P, and As. *J. Phys. Chem. A* **2015**, *119*, 1642−1656.
(130) Setiawan, D.; Kraka, E.; Cremer, D. Description of pnicogen bonding with the help of vibrational spectroscopy - The missing link between theory and experiment. *Chem. Phys. Lett.* **2014**, *614*, 136−142.
(131) Weinhold, F., Landis, C. R. *Valency and bonding: A natural bond orbital donor-acceptor perspective*; Cambridge University Press: Cambridge, U.K., 2003.
(132) Szalewicz, K. Symmetry-adapted perturbation theory of intermolecular forces. *WIREs Comput. Mol. Sci.* **2012**, *2*, 254−272.
(133) Hohenstein, E. G.; Parrish, R. M.; Sherrill, C. D.; Turney, J. M.; Schaefer, H. F., III Large-scale symmetry-adapted perturbation theory computations via density fitting and Laplace transformation techniques: Investigating the fundamental forces of DNA-intercalator interactions. *J. Chem. Phys.* **2011**, *135*, 174107.
(134) Parrish, R. M.; Sherrill, C. D. Spatial assignment of symmetry adapted perturbation theory interaction energy components: The atomic SAPT partition. *J. Chem. Phys.* **2014**, *141*, 044115.
(135) Kraka, E.; Zou, W.; Filatov, M.; Grafenstein, J.; Izotov, D.; Gauss, J.; He, Y.; Wu, A.; Konkoli, Z.; Polo, V. et al. COLOGNE2016. 2016; see http://www.smu.edu/catco (accessed Jul 31, 2017).
(136) Stanton, J. F.; Gauss, J.; Harding, M. E.; Szalay, P. G. CFOUR, A quantum chemical program package 2010; see http://www.cfour.de (accessed Jul 31, 2017).
(137) Lu, T.; Chen, F. Multiwfn: A multifunctional wavefunction analyzer. *J. Comput. Chem.* **2012**, *33*, 580−592.
(138) Werner, H. J.; Knowles, P. J.; Knizia, G.; Manby, F. R.; Schütz, M.; Celani, P.; Korona, T.; Lindh, R.; Mitrushenkov, A.; Rauhut, G. et al. MOLPRO, Version 2010. 1. A package of ab initio programs 2010; see http://www.molpro.net (accessed Jul 31, 2017).
(139) Frisch, M. J.; Trucks, G. W.; Schlegel, H. B.; Scuseria, G. E.; Robb, M. A.; Cheeseman, J. R.; Scalmani, G.; Barone, V.; Mennucci, B.; Petersson, G. A. et al. *Gaussian 09*, revision C. 1; 2010; Gaussian Inc.: Wallingford, CT.
(140) Reed, A. E.; Weinstock, R. B.; Weinhold, F. Natural population analysis. *J. Chem. Phys.* **1985**, *83*, 735−746.
(141) Bertini, V.; Dapporto, P.; Lucchesini, F.; Sega, A.; De Munno, A. 1,2,5-Telluradiazole, $C_2H_2N_2Te$. *Acta Crystallogr., Sect. C: Cryst. Struct. Commun.* **1984**, *C40*, 653−655.
(142) Freindorf, M.; Kraka, E.; Cremer, D. A comprehensive analysis of hydrogen bond interactions based on local vibrational modes. *Int. J. Quantum Chem.* **2012**, *112*, 3174−3187.
(143) Tao, Y.; Zou, W.; Jia, J.; Li, W.; Cremer, D. Different ways of hydrogen bonding in water - Why does warm water freeze faster than cold water? *J. Chem. Theory Comput.* **2017**, *13*, 55−76.

DOI: 10.1021/acs.jpca.7b06479
J. Phys. Chem. A 2017, 121, 6845−6862

(144) Kalescky, R.; Zou, W.; Kraka, E.; Cremer, D. Local vibrational modes of the water dimer - Comparison of theory and experiment. *Chem. Phys. Lett.* **2012**, *554*, 243−247.
(145) Kalescky, R.; Kraka, E.; Cremer, D. Local vibrational modes of the formic acid dimer - The strength of the double hydrogen bond. *Mol. Phys.* **2013**, *111*, 1497−1510.
(146) Zhang, X.; Dai, H.; Yan, H.; Zou, W.; Cremer, D. B-H···π interaction: A new type of nonclassical hydrogen bonding. *J. Am. Chem. Soc.* **2016**, *138*, 4334−4337.
(147) Kraka, E.; Freindorf, M.; Cremer, D. Chiral discrimination by vibrational spectroscopy utilizing local modes. *Chirality* **2013**, *25*, 185−196.
(148) Oliveira, V.; Cremer, D. Transition from metal-ligand bonding to halogen bonding involving a metal as halogen acceptor a study of Cu, Ag, Au, Pt, and Hg complexes. *Chem. Phys. Lett.* **2017**, *681*, 56−63.
(149) Setiawan, D.; Cremer, D. Super-pnicogen bonding in the radical anion of the fluorophosphine dimer. *Chem. Phys. Lett.* **2016**, *662*, 182−187.
(150) Kalescky, R.; Kraka, E.; Cremer, D. Description of aromaticity with the help of vibrational spectroscopy: Anthracene and phenanthrene. *J. Phys. Chem. A* **2014**, *118*, 223−237.
(151) Setiawan, D.; Kraka, E.; Cremer, D. Quantitative assessment of aromaticity and antiaromaticity utilizing vibrational spectroscopy. *J. Org. Chem.* **2016**, *81*, 9669−9686.
(152) Kalescky, R.; Kraka, E.; Cremer, D. New approach to tolmans electronic parameter based on local vibrational modes. *Inorg. Chem.* **2014**, *53*, 478−495.
(153) Setiawan, D.; Kalescky, R.; Kraka, E.; Cremer, D. Direct measure of metal-??ligand bonding replacing the Tolman electronic parameter. *Inorg. Chem.* **2016**, *55*, 2332−2344.
(154) Humason, A.; Zou, W.; Cremer, D. 11,11-Dimethyl-1,6-methano[10]annulene ?- An annulene with an ultralong CC bond or a fluxional molecule? *J. Phys. Chem. A* **2015**, *119*, 1666−1682.
(155) Kalescky, R.; Zou, W.; Kraka, E.; Cremer, D. Quantitative assessment of the multiplicity of carbon-halogen bonds: Carbenium and halonium ions with F, Cl, Br, I. *J. Phys. Chem. A* **2014**, *118*, 1948−1963.
(156) Kraka, E.; Cremer, D. Characterization of CF bonds with multiple-bond character: Bond lengths, stretching force constants, and bond dissociation energies. *ChemPhysChem* **2009**, *10*, 686−698.

DOI: 10.1021/acs.jpca.7b06479
J. Phys. Chem. A 2017, 121, 6845−6862